UNIVERSITY OF CALIFORNIA SAN DIEGO

Coherent Structures Sampling and a Stochastic Eddy-Diffusivity/Mass-Flux Parameterization for the Transition from Stratocumulus to Cumulus

A thesis submitted in partial satisfaction of the
requirements for the degree
Master of Science

in

Engineering Sciences (Mechanical Engineering)

by

Jiachen Lu

Committee in charge:

Professor Jan Kleissl, Chair
Professor Laurence Armi
Professor Sutanu Sakar

2019

The thesis of Jiachen Lu is approved, and it is acceptable in quality and form for publication on microfilm and electronically:

_____

_____

_____

Chair

University of California San Diego

2019

EPIGRAPH

Chance is the name we give to what we choose to ignore.

Voltaire

TABLE OF CONTENTS

LIST OF FIGURES

LIST OF TABLES

ACKNOWLEDGEMENTS

Thanks Jan Kleissl for giving me valuable advice and computational resources. Thanks Stephen de Roode for helping develop the ASTEX case and valuable instructions about the LES model. Thanks Handa Yang, Monica Zamora, Elynn Wu for introducing me to boundary layer meteorology. Thanks Paolo Davini for interesting discussions about decaying scalars and the turbulence time scale. Thanks my defense committee, Laurence Armi, Sutanu Sarkar. Thanks my family and friends for their support as always. The DALES model is available on the Github website (https://github.com/dalesteam/dales). Routines and the modified DALES used in this research are available on the Github website (https://github.com/JIACHEN427). Other model results used in the comparison together with the observation data can be found on website http://www.euclipse.nl/wp3/ASTEX_Lagrangian/LES_output.shtml

VITA

2017	B. Sc., Oil & gas storage and transportation engineering (Outstanding student), Southwest Petroleum University, Chengdu, China
2019	M. Sc., Engineering Sciences (Mechanical Engineering), University of California San Diego

ABSTRACT OF THE THESIS

Coherent Structures Sampling and a Stochastic Eddy-Diffusivity/Mass-Flux Parameterization for the Transition from Stratocumulus to Cumulus

by

Jiachen Lu

Master of Science in Engineering Sciences (Mechanical Engineering)

University of California San Diego, 2019

Professor Jan Kleissl, Chair

The transition from stratocumulus (Sc) cloud to cumulus (Cu) cloud occurs when air parcels advect from subtropical ocean to tropical ocean. Due to complex physics involved during the transition, it is hard to represent it in large/meso-scale models and the transition itself is crucial to the energy budget for the subtropic environment. The Atlantic Stratocumulus Transition Experiment (ASTEX) was conducted specifically to resolve this problem. In this research, ASTEX case was simulated with Dutch Atmosphere Large Eddy Simulation (DALES) model with two decaying scalars designed to track the origination of air parcels. During 40 hours of simulation for ASTEX, the decoupling stage accounted

for 30 hours, showing a clear three-layer-structure: i) a well-mixed surface layer driven by surface heating; ii) a Cu layer with heating and moisture feeding from the surface and cooling and drying from the Sc layer but without sufficient turbulent kinetic energy (TKE) to mixed them together; iii) a well-mixed Sc layer driven by radiative cooling. During the transition, Sc layer becomes thinner and the downward non-local mixing becomes weaker, which further promotes the decoupling.

To help build a clear representation of the Sc-Cu transition in the Numerical Weather Prediction model (NWP), a quadrant analysis based on a decaying scalar and vertical velocity perturbation with vertical velocity probability density function (wPDF) filter was used separating the turbulent shell and coherent structures. A clear dynamic cycle among turbulent shells and interactions between the turbulent shells and coherent structures was observed. To show the gradual decrease of the vertical mixing within Sc layer during transition, a comparable downdraft initiated from cloud base was added to the existing state-of-art stochastic Eddy-diffusivity Mass-flux (EDMF) planetary boundary layer (PBL) parameterization.

Chapter 1

Introduction

1.1 Motivation

Stratocumulus (Sc) cloud is the most common cloud type on the Earth. It covers about 20% of the Earth surface in the annual mean and represents a large source of uncertainty in global climate model simulations [Wood, 2012]. Because the liquid water content largely determines its optical properties, the cloud dynamics and its radiative properties are closely linked and important for Earth's energy budget through their reflection of solar radiation and reduction of longwave radiative heat losses.

Parameterization of the separate cumulus (Cu) and stratocumulus boundary layer is widely studied [Siebesma et al., 2007, Neggers, 2009, Handa, 2018], with several attempts to unify the Cu parameterization and Sc parameterization. [Bechtold et al., 1995, Chung et al., 2012, Leeuwen, 2014], yield a good result. The eddy-diffusivity (ED) approach proves to be relatively successful for stable convective stratocumulus-topped boundary layer (STBL), so the turbulent transport in STBL is often parameterized by the ED parameterization. Since ED schemes have difficulties in representing shallow convection and may produce incorrect mixing in the cloud layer, a combined advec-

tion–diffusion decomposition scheme called Eddy-diffusivity/Mass-flux (EDMF) scheme [SOARES et al., 2004, Siebesma et al., 2007] is often used. Mass-flux (MF) schemes are well-suited for the Cu-topped BL, where mass flux represents a bulk updraft; the heat and water transport in cumulus cloud layers is most often parameterized with MF parameterization. In the Barbados Oceanographic and Meteorological Experiment (BOMEX) case, MF contribution in the heat and water transport budget represents 60 to 90% of the total vertical moisture and heat transport in the cumulus cloud layer.

To study the unified parameterization for transition from Cu to Sc, Atlantic Stratocumulus Transition Experiment (ASTEX [Albrecht et al., 1995]) was conducted with Lagrangian [Leeuwen, 2014] or Eulerian [Chung et al., 2012] view. During the ASTEX, aircraft observations of a transition from a solid stratocumulus topped boundary layer to a boundary layer dominated by shallow cumulus clouds penetrating a thin veil of broken stratocumulus were collected. [van der Dussen et al., 2013]. Figure 1.1 shows 5 experimental flights during the first Lagrangian ASTEX with start/end site labeled. The first analysis was performed [Bretherton and Wyant, 1997, Stevens, 2000] with low resolution, focusing on finding a critical value for the decoupling to happen by using buoyancy flux integral relationship [Wood and Bretherton, 2004]. [Sandu et al., 2010, Van Der Dussen et al., 2016] designed several composite cases with designated large scale forcings (sea surface temperature (SST) and large scale subsidence) to test the major factors that control the thinning of Sc and the transition from Sc to Cu. [Chung et al., 2012] performed several steady transition cases with a similar setup as in ASTEX but with fixed large scale forcings and SST. This simplifies the investigation of cloud response without the inherent time-lag effects in a transient transition case but maintains a less direct relationship to the actual evolution of the boundary layer. [Leeuwen, 2014] Performed the real ASTEX simulation with Dutch Atmosphere Large Eddy Simulation (DALES [Heus et al., 2010]) and proposed a new dual EDMF parameterization scheme for the subcloud layer defined by the vertical

velocity skewness and the cloud layer separately.

1.2 Coherent structures and transition

In the study of turbulence, coherent structures (CS) are regions of space and time significantly larger than the smallest flow or turbulence scales within which the flow field has a characteristic coherent pattern [Pope, 2000, ROODE and DUYNKERKE, 2004]. However, for the specific objective of the study, CS have a different definition. For atmospheric science, the organized, large scale air motion as oppose to the small scale turbulence shells (TS) is often called convective structures or plumes, which is a key element of the PBL and responsible for the turbulent vertical transport of heat, momentum and trace species, via a non-local transport and often can be classified as updrafts, downdrafts, subsiding and ascending shell. In numerical weather prediction models (NWP), these structures are not explicitly resolved and must be parametrized. Several attempts have been made from aircraft measurements [Young, 1988] and other instruments such as radar, [Chandra et al., 2010]. In addition to observations, LES that resolves explicitly air motions with scales larger than $\sim$ 5m to $\sim$ 50m, depending on the resolution, provides more detailed cloud and convective process with 3D field values of variables of interest and have been widely used to generate relatively real data to seek for parameterization in NWP models. It is still not trivial to isolate the CS [Siebesma and Cuijpers, 1995] from LES results with the highly chaotic nature of turbulence. [Berg and Stull, 2004] reviewed three different sampling criteria used to sample CS.

1. *Indicator variables to define the thermal.* With the presence of liquid water (q_l), several other thermodynamic variables such as liquid water potential temperature (θ_l) and total water mixing ratio (q_t) that conserve for adiabatic lifting and condensation/evaporation of water, virtual potential temperature (θ_v) that represents the buoy-

ancy, and perturbation vertical velocity with respect to the slab average ($w' = w - \overline{w}$), with overline indicate the slab average. The current trend of using the variables focus on introducing passive tracer; [Couvreux et al., 2010] used a combination of a passive tracer emitted at the surface and thermodynamic variables to characterize organized structures in large-eddy simulations. [Park et al., 2016, Davini et al., 2017] introduced an additional scalar to trace air from the free troposphere, together with a scalar resembles the stratified boundary layer, performed an octant analysis for 8 different octants.

2. *Some threshold value of the indicator variable.* e.g. [Greenhut and Khalsa, 1982]

3. *Some length scale.* Since CS should be coherent within a certain length scale, with turbulence spectra the scale for specific air motion can be sampled.

This work is the first half of research aimed to improve the physical modeling of transition from Sc to Cu in the (NWP) model. To account for the gradual weakening of the downward non-local turbulent transport within the cloud layer during transition two major modifications on the state-of-art stochastic parameterization [Sušelj et al., 2013] were made: i) a downdraft initialized from the Sc base is introduced with the same vertical velocity budget and later entrainment but without the condensation; ii) with a new way of conditional sampling technique of CS adapted from [Davini et al., 2017] by introducing two passive and decaying scalars, a dynamic cycle between the turbulent shells (TS) and CS, CS is found to only have interactions with its paired TS, which indicates the actual later entrainment is weaker than previously studied. To resolve this problem, the lateral entrainment was designed to only from the turbulent shells instead of the environment.

The organization of the present study is as follows: LES setup and results from two simulation with different resolution in Chapter 2; conclusion and discussion are given in chapter 5; basic theory and the new approach are proposed in Chapter 3. Finally, with

the plume properties acquired, implications of potential modifications of the state-of-art stochastic EDMF scheme is described in Appendix 4.

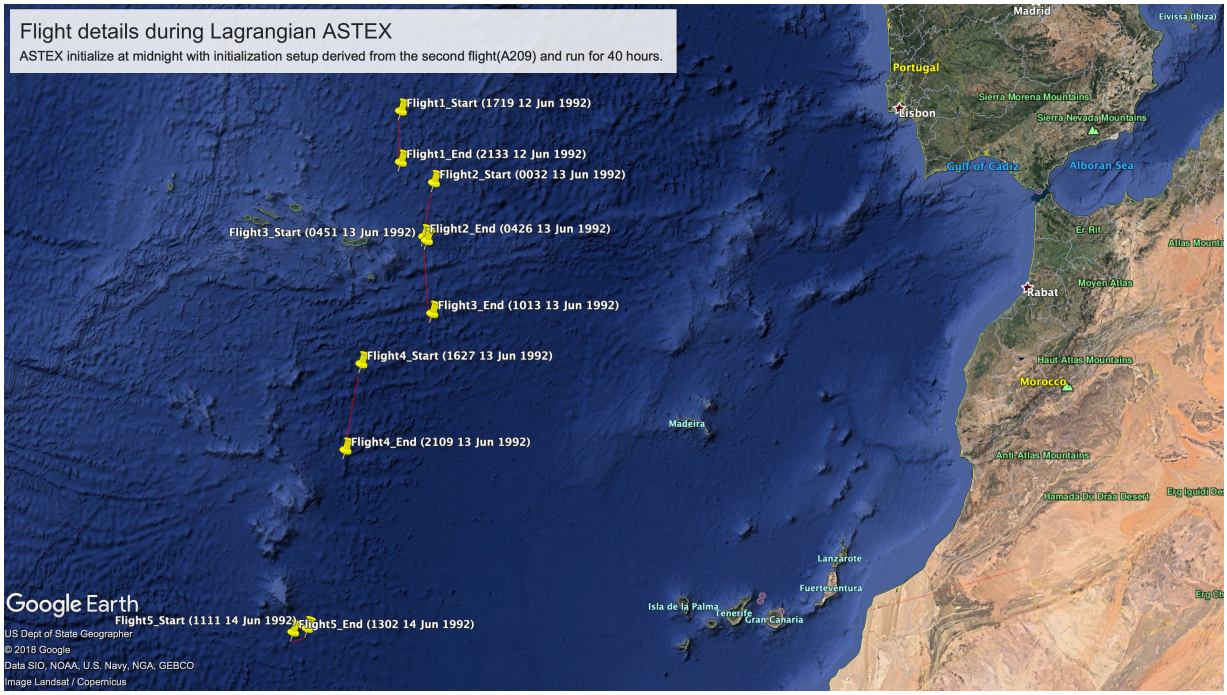

Figure 1.1: Flight details during ASTEX. The ASTEX simulation is initialized from the second flight (initialization). the third flight (hour 8), fourth flight (hour 19), fifth (hour 36) [van der Dussen et al., 2013], image from Google Earth.

Chapter 2

Design of numerical experiments and results

2.1 EUCLIPSE model intercomparison revisit – Why DALES

In the long history of studying the ASTEX case, University of California Los Angeles Large Eddy Simulation (UCLALES) [Chung et al., 2012] model and DALES model [van der Dussen, 2014] are the main two popular models to run. To compare which one is more favorable, European Union Cloud Intercomparison, Process Study & Evaluation Project (EUCLIPSE) intercomparison [van der Dussen et al., 2013] is a good place to look. The model intercomparison for ASTEX case with results from EUCLIPSE website [1] in Figure 2.1 shows the total water mixing ratio (q_t) and liquid water potential temperature (θ_l) with each hour piled together from DALES, EULAG, UCLALES, MOLEM, SAM, DHARMA model. Because the linearly growing SST and the large scale subsidence, the PBL height will grow deeper from $\sim$ 600m to $\sim$ 2000m, but instabilities can be found

[1] http://www.euclipse.nl/wp3/LES_Data/ASTEX/

propagating from the top boundary to the inversion height in the UCLALES, MOLEM and SAM model (red squared), especially for total water mixing ratio q_t. This instabilities could have devastating effects when running a longer simulation that allows these instabilities to propagate low enough and PBL height to grow deep enough (the instability will merge with the inversion, and the inversion height is often determined by the gradient of variables, contaminated inversion gives bad estimate of the inversion height, which is a critical diagnostic variable). In tests run with UCLALES, these concerns become real and cannot be resolved; a good guess for this instability would be the inappropriate radiation scheme or profile. In contrast, DALES shares a lot of features with UCLALES without this kind of issue, which makes it a favorable model to switch to run ASTEX among models presented in the EUCLIPSE intercomparison campaign.

2.2 LES Model Setup

Most of the model setup follows EUCLIPSE campaign[2]. Because a different version of DALES and a different resolution are used, further validation of the result is necessary and will be shown in the next section.

- **Grid setup** — One case with resolution 427×128×128 (*nonequi*) with nonequidistant vertical grid (finer at the inversion range (600m∼2400m), above 2400 serve as the gravity damping layer. Field results are saved at every 600s to get the result for time evolution. Another case has a resolution of 200×512×512 (*equi*) with initial setup derived from the nonequidistant case to have more horizontal resolution with limited memory and computation resource. Field results are saved at every 3600s to get the field details. Both of them covers 4480m×4480m×3048m space, The resolution of (*equi*) is 15.24m×8.75m×8.75m.

[2]http://www.euclipse.nl/wp3/ASTEX_Lagrangian/LES_astex_setup.shtml

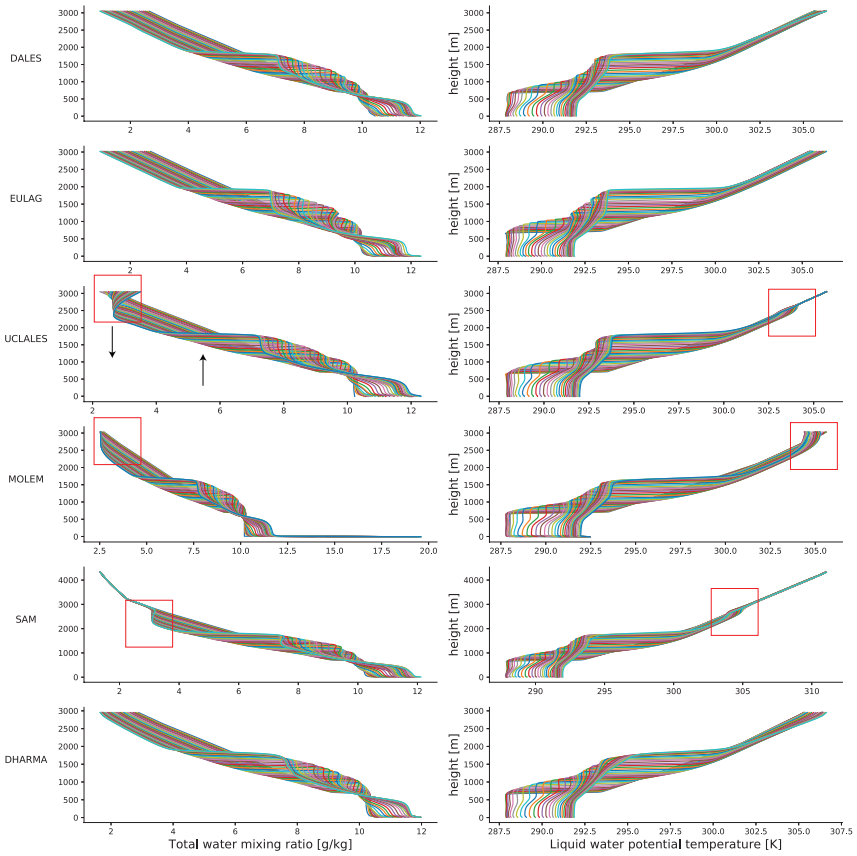

Figure 2.1: Slab-averag total water mixing ratio and liquid water potential temperature, instabilities can be found at top boundary in the UCLALES, SAM and MOLEM model (red squared), note that the inversion height is growing up and the instabilities is propagating down (black arrow)

- **Radiation scheme** — RRTMG [Hu and Stamnes, 1993, Iacono et al., 2008] or Fu-Liou scheme [Fu and Liou, 1993].

- **Surface scheme** — Forced surface temperature, moisture/temperature fluxes are calculated.

- **Microphysics scheme** — Bulk microphysics implemented by introducing two additional scalars. [Kogan, 2013]

- **Advection scheme** — Advection with 5th order upwind scheme and 2nd order in the vertical for all the diagnostic variables except the momentum with 2nd order

central differencing scheme. [Jiang and Shu, 1996]

- **Time integration** — 3rd order Runge Kutta time integration with adaptive time step according to the Courant number and the cell Peclet number.

- **Decaying scalars** — The same setup as in [Davini et al., 2017], except with an adaptive relaxation time scale and profile for S_{FT}. Detailed discussion in the next chapter.

- **Large scale forcing** — ASTEX case observed air parcel is part of the tradewinds. The tradewinds themselves are part of a planetary atmospheric circulation cell, which is called the Hadley cycle is shown in Figure 2.2. The large scale forcing is the major cause of cloud decoupling and the transition from STBL to trade wind cumulus. [Chung et al., 2012] ran several simulations with fixed large scale forcings, but in this research, to get a more realistic result, a linearly growing SST and large scale subsidence rate are used. Since the flight is equatorwards, the large scale forcings can be set as follows:

  1. **Sea surface temperature** SST is growing from 291 to 297K linearly, SST variation is presented by liquid water potential temperature at the surface.
  2. **Large scale subsidence rate** Prescribed large-scale subsidence profile.

$$\overline{w}(z) = \begin{cases} -Dz & \text{for } z \leq z_D, \\ -Dz_D & \text{otherwise} \end{cases} \tag{2.1}$$

  Where D is the large-scale divergence of horizontal winds and grows linearly, z_D here is 1600m.

- **Subgrid-scale turbulence** [Deardorff, 1980]

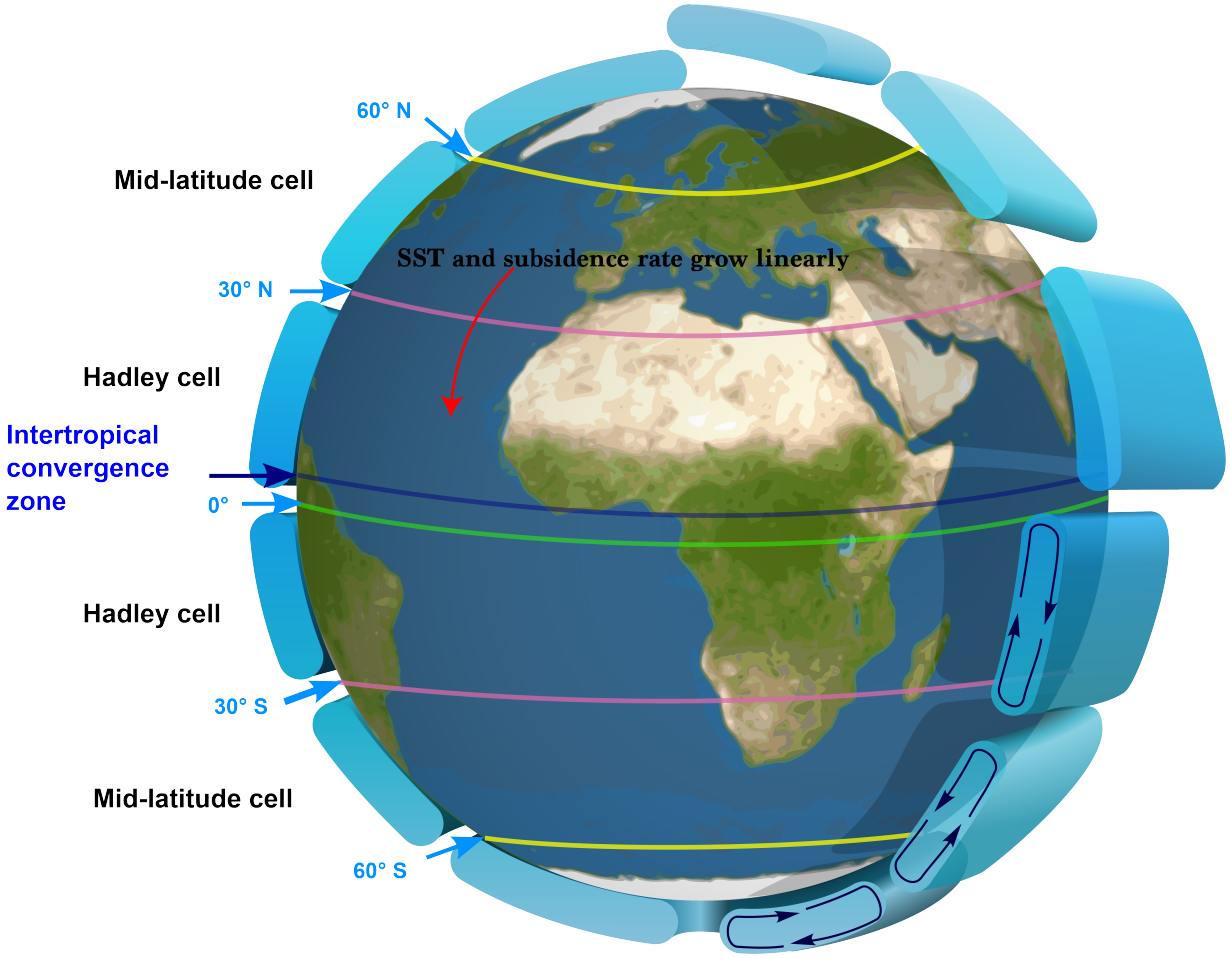

Figure 2.2: Hadley cells with the global circulation, the air parcel advection direction is labeled as red arrow, figure from Wikipedia.

2.3 Physics during Transition

In this section, results from LES simulation along with comparisons with other models presented at EUCLIPSE intercomparison are shown. Note that because of the different case setup for ASTEX and different version of DALES, the original result is labeled as DALES_DUSSEN, while the result in this research is labeled as DALES_MOD. Since observations are made approximately at the initialization and 8th/19th/36th hour, [van der Dussen et al., 2013], we choose them mainly for discussion and validation. With the major cloud type found during ASTEX, the transition is divided to three stages, which

are **stratocumulus** stage (0-8 hour), **stratocumulus-cumulus** stage (8-36 hour) and **cumulus** stage (36-40 hour). The 3D cloud field can be seen in Figure 2.3

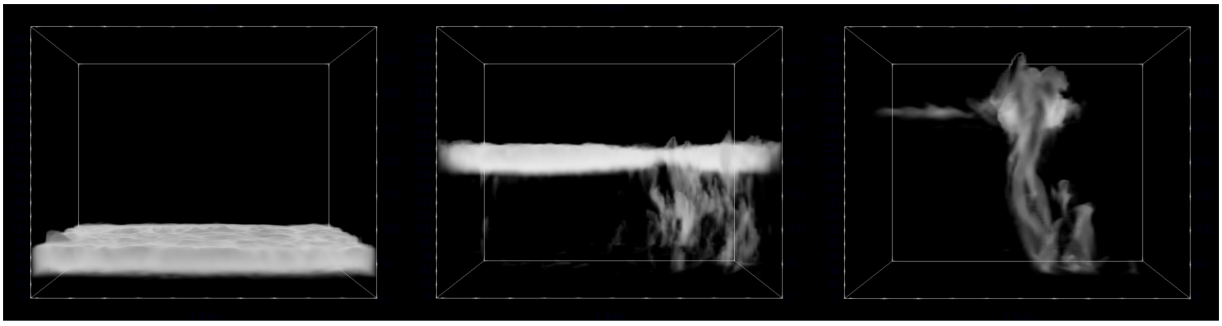

Figure 2.3: 3D cloud field in 3 stages, the liquid water content is used to show the cloud.

2.3.1 Vertical profiles

This section shows the vertical profiles of related variables in this research with results from other models and observation. Note that the last 27 sponge layers are excluded for the result output; only 400 vertical grids are shown here.

Figure 2.5 shows the slab-average vertical profiles of the conserved variables in various models. As the air parcel advects to the equator and inversion height grows higher, the surface moisture content and temperature grows larger indicating the transition of subtropical ocean to tropical ocean. TKE is generated by surface heating at the initialization stage, temperature and moisture content are both well-mixed below the inversion height indicating a well-coupled boundary layer. Above it, the profile follows the lapse rate of each variables. At the 19th hour, as stated in Section 1.2, insufficient turbulent kinetic energy results in 3 layers. The surface layer and Sc layer are still well-mixed but have already decoupled and separated by a Cu layer. Figure 2.4 shows the physical process during the decoupling stage.

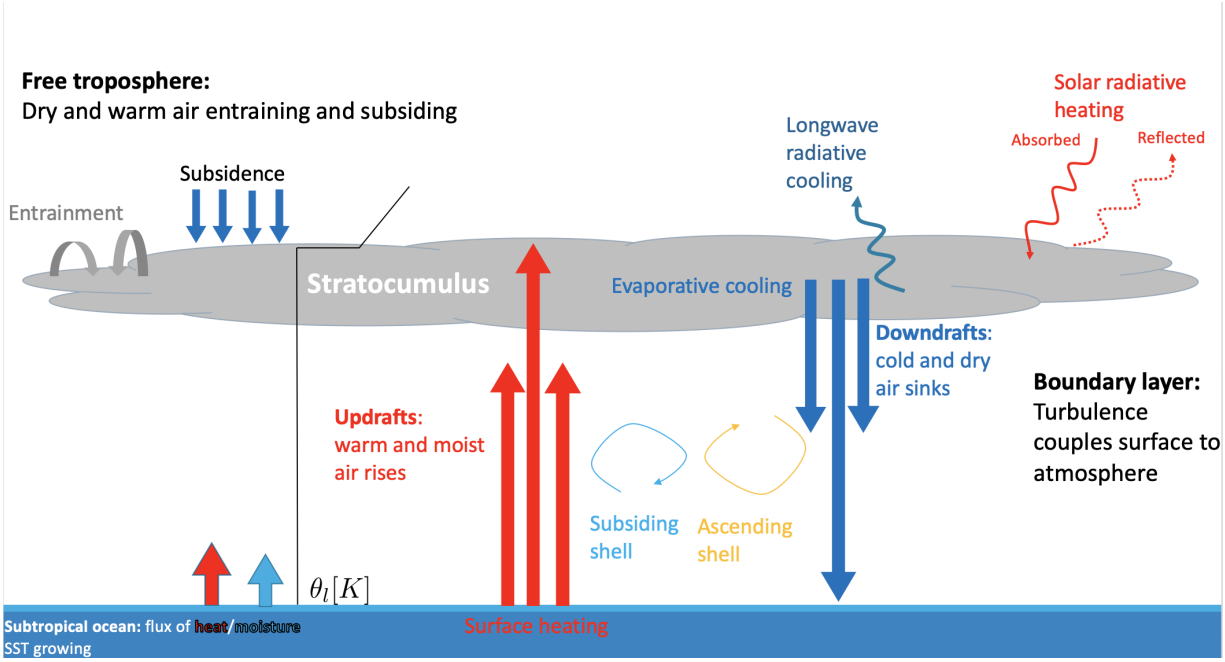

Figure 2.4: Physical process during the decoupling stage. The three-layer-structure can be seen in the θ_l vertical profile.

Figure 2.6 shows the vertical velocity variance and normalized vertical velocity skewness. Variance of vertical velocity is an important indicator for stratification within PBL. For 19th hour, the two-parabolic shapes indicate strong vertical mixing from both side(surface heating for surface layer, radiative cooling for Sc layer.

2.3.2 Time evolution

In Figure 2.7, the stratocumulus cloud layer is defined as cloud fraction $\sigma_c > 0.4$. As the air parcels advect to the equator, this layer becomes thinner and grows deeper. The layer below Sc and above the cloud base is defined as cumulus layer, surface layer is defined as area below the cloud base. Finally, the Sc layer vanishes for the last 4 hours, leaving a Cu layer and results in abrupt decrease of the cloud fraction. The cloud fraction at observation time points are shown. While the height of maximum cloud fraction is growing, the height of the second maximum of cloud fraction persists during simulation

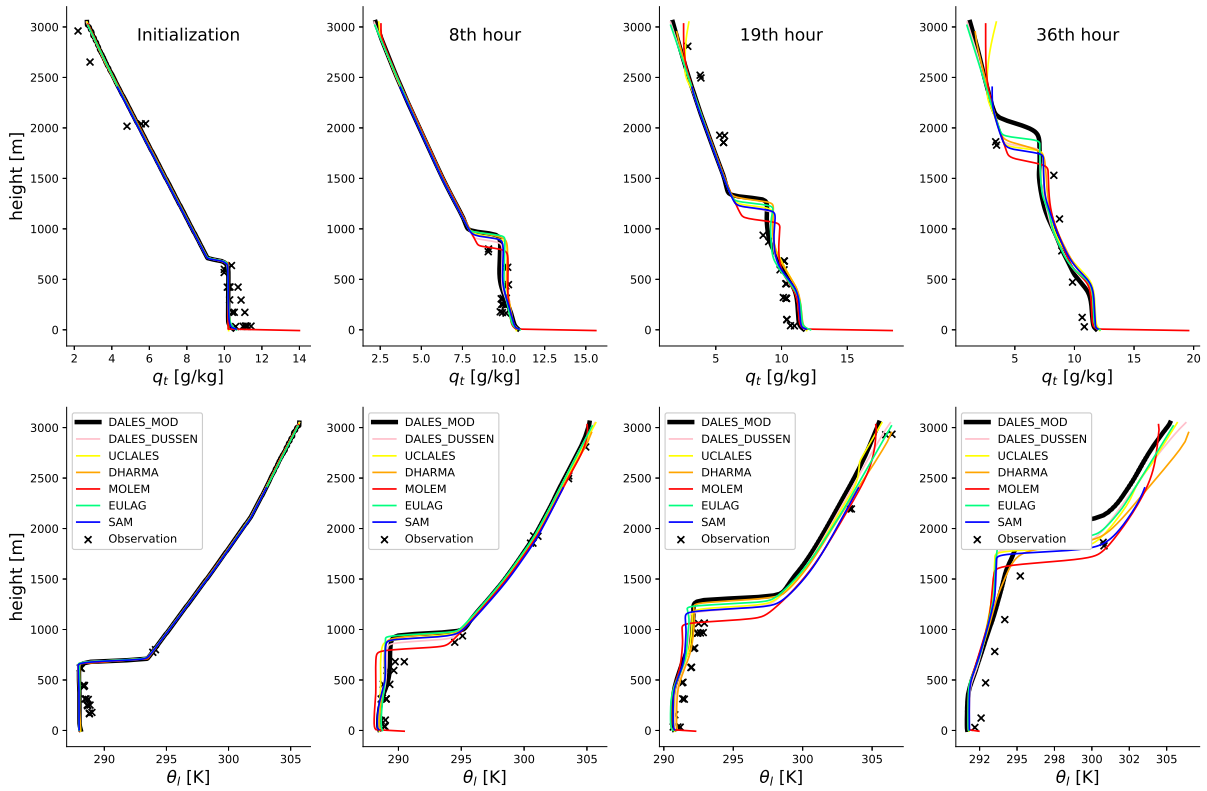

Figure 2.5: Slab-average of moist conserved variables (total water mixing ratio (top), liquid water mixing ratio (bottom)) with different models, observed value at estimated time show with black cross.

and is defined as subcloud height.

Figure 2.8 shows the time evolution of concerned variables in this simulation and others presented in the EUCLIPSE intercomparison. The upper left shows a monotonically growing cloud top and relatively stable cloud base. The liquid water path, which is the vertical integration of liquid water content grows for the first few hours before the sunrise and decreases with aggravated speed for the rest of the day. After the first sunset, the temperature of all the air parcels decreases and prompts more condensation and more liquid water. Together with other large scale forcings caused by equatorwards advected cumulus, the LWP is maintained during the second night. After the second sunrise, the condensation was inhibited and the LWP decreased again. The cloud fraction is maintained

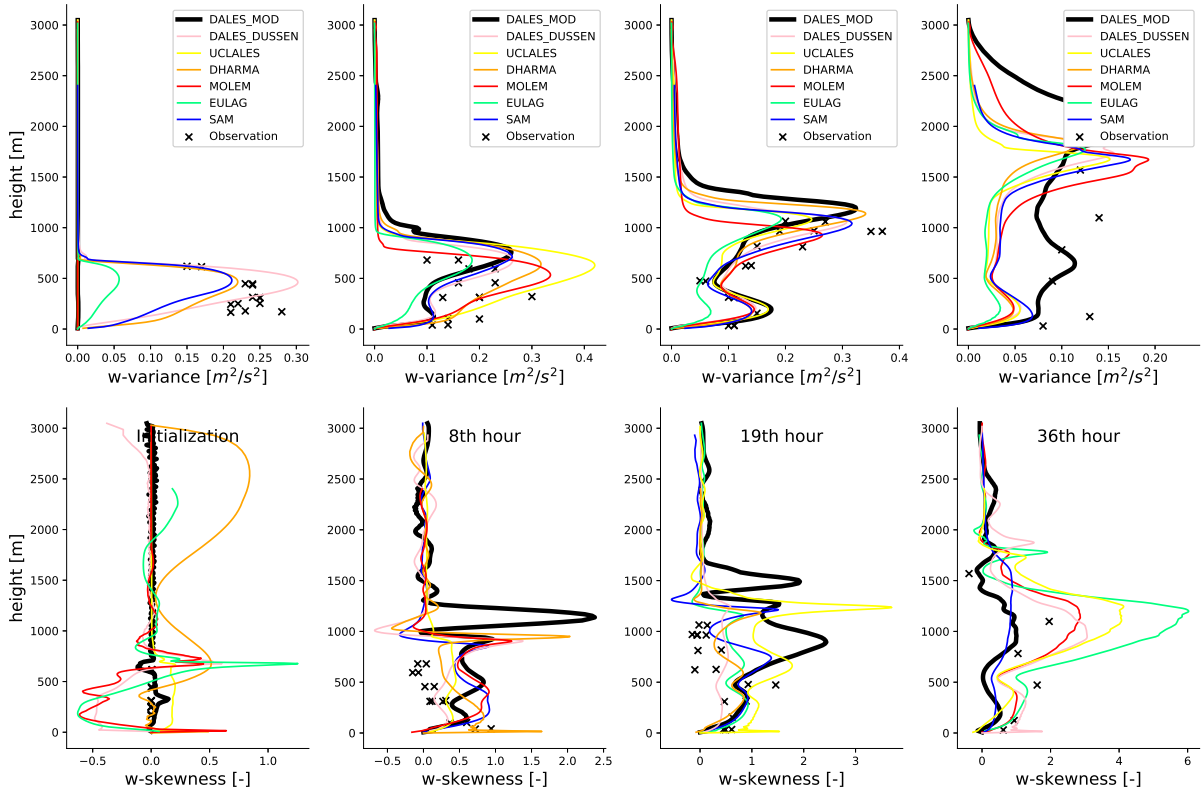

Figure 2.6: Vertical velocity variance ($w'w'$, top), a decoupled boundary layer can be observed with two separated parabolic curves. And normalized vertical velocity skewness calculated with $skewness = w'^3/(w'^2)^{3/2}$ (bottom)

for the first 30 hours but decreased abruptly after because of the breaking of the very thin Sc. Bowen ratio, which is defined as ratio of surface sensible heat flux (surface kinematic temperature flux) and surface latent heat flux (surface kinematic moisture flux) indicates the changing of the sea surface from subtropical ocean to tropical ocean and it is the main cause of the transition.

2.3.3 Instantaneous Cross section

Figure 2.9, 2.10, 2.11 show instantaneous cross sections of liquid water content and other three variables used to do the quadrant/octant analysis for three stages. The liquid water content can represent the cloudy air parcel. At Sc stage the Sc cloud is still thick,

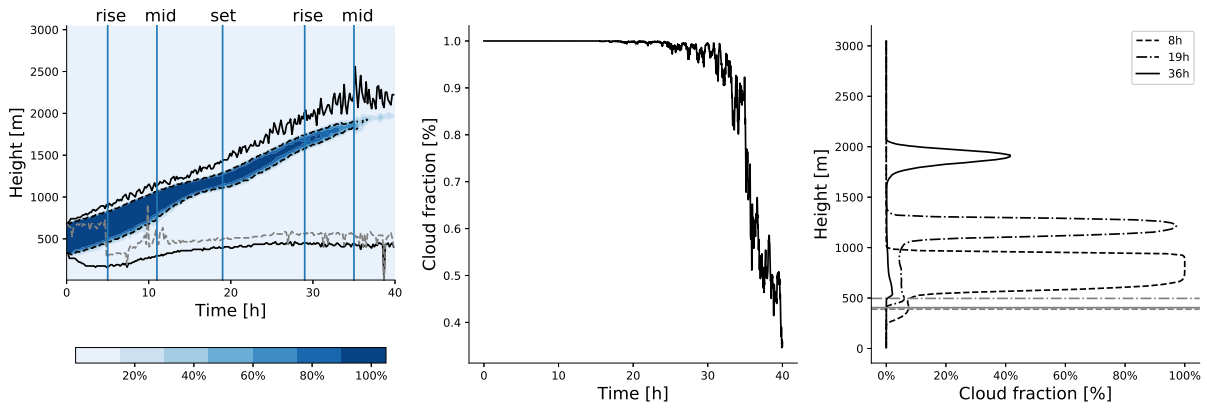

Figure 2.7: Evolution of cloud top/base and stratocumulus top/base defined as $\sigma_c > 0.4$ and subcloud height defined as the height with second maximum cloud fraction (left), cloud fraction (middle), cloud fraction profile and corresponding subcloud height (right).

but a crack can be clearly seen in the q_l plot. A corresponding large portion of S_{FT} can be observed, which is an indicator of the entrainment events. The vertical velocity indicates the origin of the vertical mixing; it is clear that the vertical velocity source originates from both sides while the middle layer has relatively horizontal velocity, causing the decoupling of the boundary layer. During the decoupling stage vertical velocity Figure 2.10 shows a clear three-layer-structure where the upper Sc layer and lower surface layer is with relatively large perturbation compared to the middle Cu layer. The Sc layer is largely thinned due to insufficient moisture feeding and increased entrainment due to increased environment temperature. At the final Cu stage, the Sc layer is fully dissolved, leaving only a trade wind cumulus layer, and vertical turbulence becomes much smaller than before.

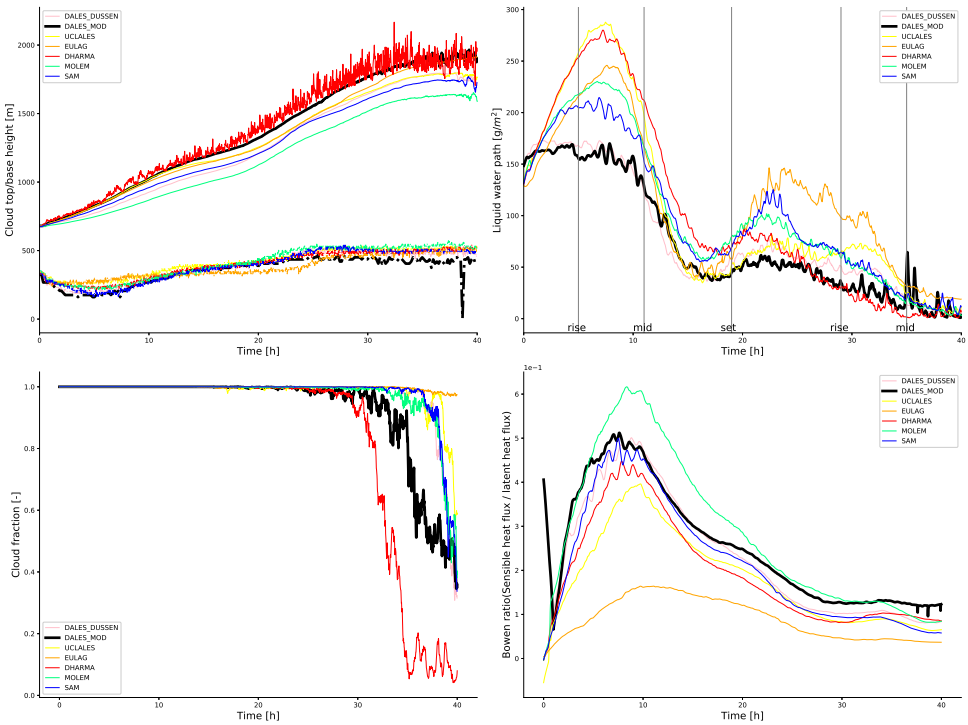

Figure 2.8: Time evolution of the cloud top/base (top left), liquid water path (top right, calculated as $LWP(z) = \int_0^{zi} \rho_{air} q_l dz$), cloud fraction TKE (bottom left), Bowen ratio (bottom right).

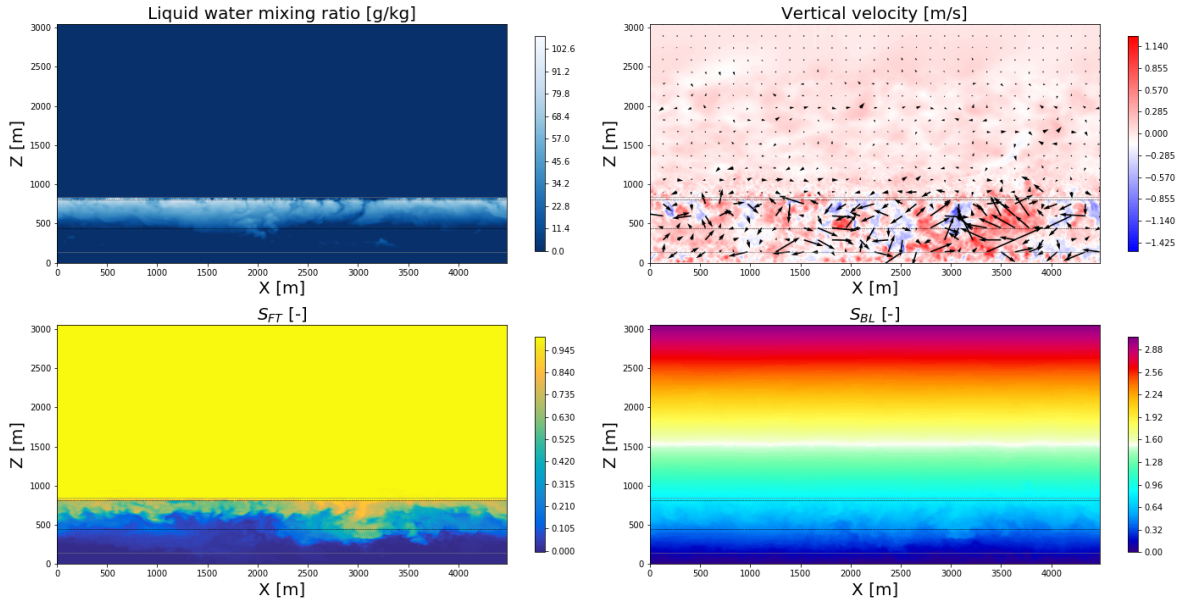

Figure 2.9: Cross section properties at the beginning hour 4 for liquid water mixing ratio (top left), vertical velocity with velocity direction indicated by black arrows (top right), S_{FT} (bottom left) and S_{BL} (bottom right) **(Stratocumulus stage)**.

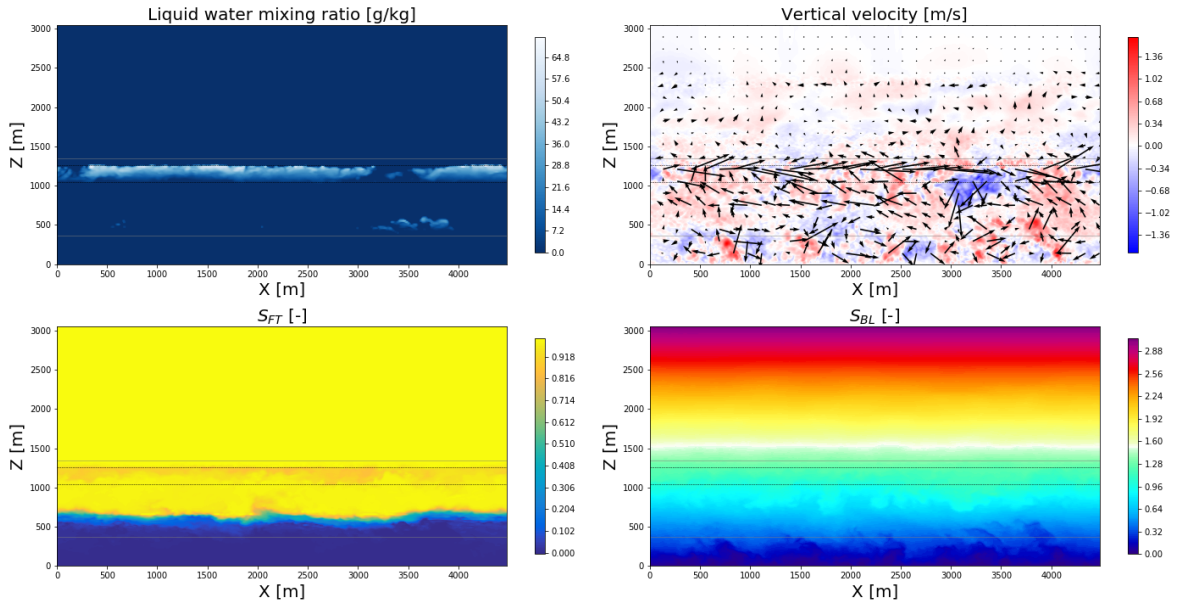

Figure 2.10: Cross section properties at the beginning of hour 19. (**Decoupling stage**)

.

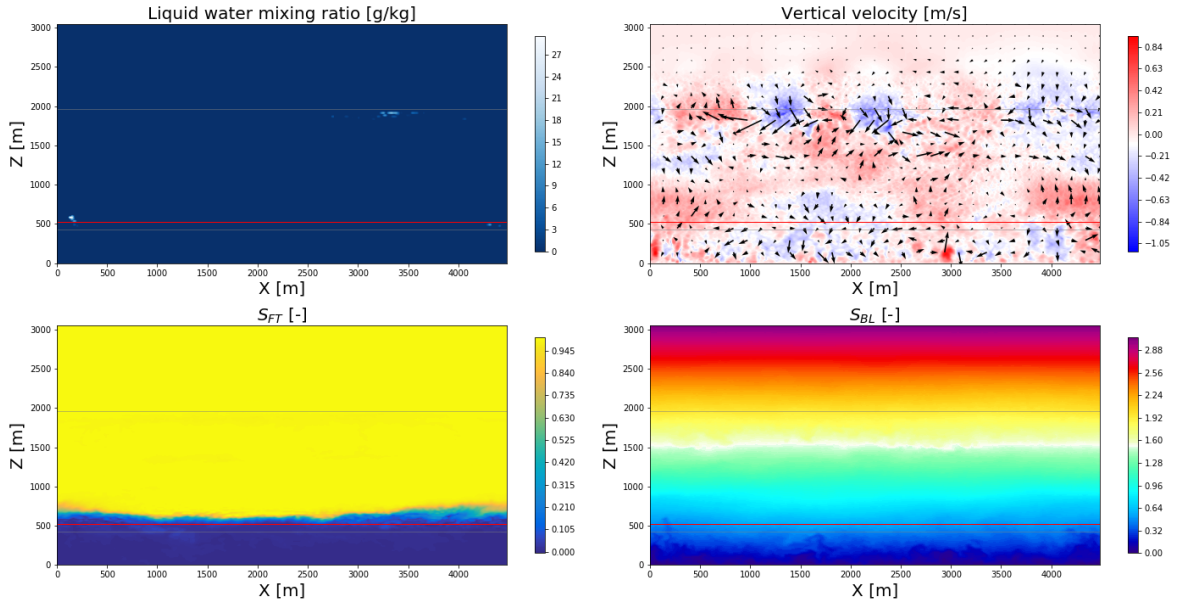

Figure 2.11: Cross section properties at the beginning of hour 38. (**Cumulus stage**)

.

Chapter 3

Conditional sampling of coherent structures

CS are large-scale structures in the turbulent flow that have similar thermodynamic characteristics within certain spatial or temporal range. They are responsible for the non-local turbulent transport opposed to the local turbulent transport TS did. Modern PBL parameterization schemes usually consider the CS and TS separately [Neggers, 2009, Sušelj et al., 2013, Berg and Stull, 2004], and use plume properties diagnosed from LES to fit parameters in their model. To capture CS, often liquid water potential temperature (θ_l) and total water mixing ratio (q_t) [KUANG and BRETHERTON, 2006] are used, but since they are highly correlated, sampling the coherent structures using these tracers can be misleading [Park et al., 2016]. Also, using liquid water also has limitation for area below the lifting condensation level and cannot deal with the cumulus stage as in Figure 2.11. [Siebesma et al., 2007, Leeuwen, 2014] used percentile of probability density function (%PDF) of vertical velocity to sample updraft, which as a consequence result in a fixed updraft fraction and may vary a lot among different case and requires further discussion case by case. Traditional sampling criteria often only separate the updraft

and environment with the downdraft considered by the eddy diffusivity part, while the effects of downdrafts and entrainments are comparable to the effects of updrafts in STBL [Handa, 2018]. As concluded in Chapter 2, clear representation of the downdraft maybe is a key part to reconstruct the Sc-Cu transition in the NWP model.

3.1 Two decaying scalars

In traditional sampling, there are three types of scalars that are involved in the atmosphere numerical simulation. The relation of active/passive scalar to the velocity field in turbulence flow can be shown as:

$$\frac{\partial a}{\partial t} + v\nabla a = \kappa_a \Delta a + \mathcal{F}_a \quad a \in (q_t, \theta_l, \dots), \tag{3.1}$$

$$\frac{\partial v}{\partial t} + v\nabla v = -\nabla p + \nu \Delta v + \mathcal{F}(a, \nabla a, \dots), \tag{3.2}$$

$$\frac{\partial c}{\partial t} + v\nabla c = \kappa_p \Delta c + \mathcal{F}_c \quad c \in (S_{BL}, S_{FT}, \dots) \tag{3.3}$$

where $\frac{\partial}{\partial t}$ denotes the tendency of scalars. The second term in each equation represents the advection/convection. Subscript a represents the active scalars such as water vapor/liquid/ice mixing ratio or liquid water potential/virtual temperature, v represent the velocity scalars in three directions. Subscript c represents passive scalars such as some chemical species and the two additional scalars introduced in this research. κ and ν are the diffusivity for scalars and viscosity for momentum, $\mathcal{F}$ is the source/sink term for these three types of scalars. Active scalars have two-way interaction with the velocity field since they advect with air and affect the velocity field by modifications on the sink/source term.

For passive scalars, they only have one-way interactions with velocity fields by advection and have no modifications on it. From sensitivity tests in [Davini et al., 2017], we know the surface flux doesn't affects the result significantly, so we set no surface flux

and no large scale forcing for the scalars. This leaves us with a rather simple physical process with only diffusion and advection. Still, the large scale forcing can affect scalars by indirect effects on the velocity field. Since periodic boundary conditions are used in the horizontal directions (what is entering on the left boundary is given the propeties of what left at the other side and vice versa), passive scalars are conserved for all the physical processes happening in the simulation, which makes them ideal tracers for air motion, and capable of recording the history of the velocity field.

Follows [Davini et al., 2017], S_{BL} is designed with a monotonically growing profile $S_{BL} = z/1000$, which resembles a stably stratified atmospheric layer. S_{FT} is zero below the initial inversion height and unity above it, which is used to detect the slower process associated with free-tropospheric entrainment. Figure 3.1 shows the vertical grid for the non-equidistant simulation and initial profiles of two decaying scalars during ASTEX.

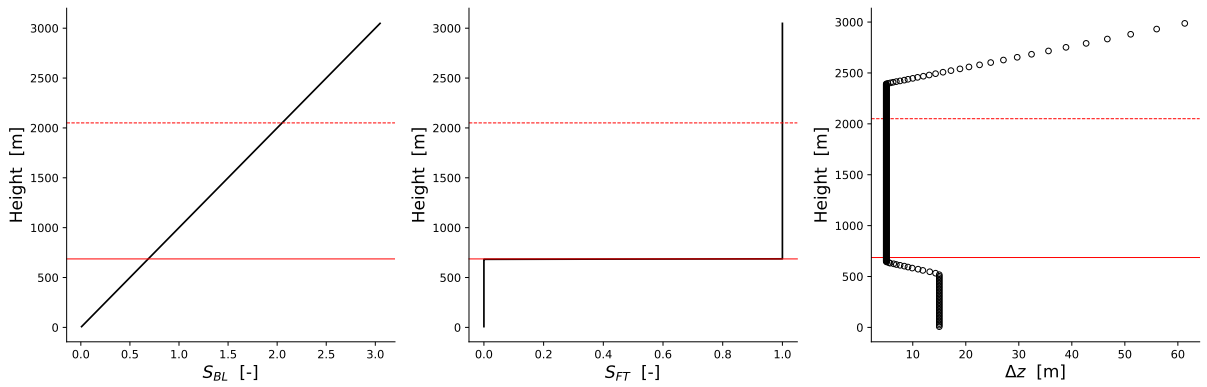

Figure 3.1: Initial profile for S_{BL} (left), S_{FT} (middle) and vertical grid setup for the *nonequi* run (right). Solid red line represents the initial inversion height, dash red line represents the final inversion height, vertical grid is made finer to catch the inversion height more precisely.

Table 3.1 shows the three variables used to do the octant decomposition of the air parcel in the PBL. Air parcels are divided by two decaying scalars introduced above and the vertical velocity perturbation, which indicates the current direction of motion of air parcels with respect to the horizontal mean. S'_{BL} indicates the origination of air parcels.

$S'_{BL} < 0$ indicates that air parcels with lower value of S_{BL} have been transported upward and renders its value to current grid. In the same sense, $S'_{BL} > 0$ indicates air coming from above. With these two indicators, when air parcel moves downwards ($w' < 0$) and originated from upper level, this is defined as the downdraft. When the air parcels move upwards ($w' > 0$) and originated from lower level, this is defined as the updraft. The other two quadrants, with the same sign of these two indicators, define turbulent shells, which change their transport direction representing short-time fluctuations. The turbulent shells with positive vertical velocity perturbation, define the ascending shell; with negative defines the subsiding shell. Unlike S_{BL}, using S'_{FT} can be misleading. Duo to the lower level of the PBL, the air parcel with small positive S_{FT} compared to smaller slab-average values would be spuriously considered as entrainment. As a result, a threshold should be found to be used to maximize the difference of the downdraft and entrainment, which are the two major coherent structures and responsible for most part of turbulence transport at the cloud layer. Then the processed value $S^*_{FT} = S_{FT} - thr$ can be used in the octant analysis. A cost function based on that is developed in [Davini et al., 2017] to determine the threshold instead of the slab-average value.

$$\mathrm{CF(thr)} = \int_0^{z_{top}} \overline{w'\theta'}_{l,\ \mathrm{down}} dz - \int_0^{z_{top}} \overline{w'\theta'}_{l,\ \mathrm{entr}} dz \tag{3.4}$$

Where the first term of this equation is the integral of vertical heat flux of the downdraft octant, and the second is for the entrainment octant. The threshold can be attained by iteratively updating the *thr* to maximize the cost function. Any air parcel with S^*_{FT} further divided the air parcels to air motion result from the entrainment related motions and motions within PBL.

Since there is no source/sink term assigned to passive scalars during simulation, like dyes in water, scalars will be well-mixed and become useless after several hours of simulation. As a result, a decaying mechanism is introduced to relax them to their original

Table 3.1: Octant definition based on the sign of perturbation of vertical velocity and S_{BL} with S_{Ft} minus the threshold that maximize the difference of vertical integral of the turbulent heat flux, only entrainment shown after using S^*_{FT}.

	Octant							
	1	2	3	4	5	6	7	8
S^*_{FT}	+	+	−	−	+	+	−	−
S'_{BL}	+	−	+	−	+	−	+	−
w'	+	+	+	+	−	−	−	−
Name	-	-	Ascending shell	Updraft	Entrainment	-	Downdraft	Subsiding shell

value to avoid the formation of a well-mixed region in the boundary layer and prevents downward accumulation while capturing top-down motions and maintaining a quasi-steady mean state [Park et al., 2016]. The equation governing the relaxation read as follows.

$$\frac{\partial S_{BL}}{\partial t} = -\frac{S_{BL} - z/1000}{\tau_{BL}}, \tag{3.5}$$

$$\frac{\partial S_{FT}}{\partial t} = -\frac{S_{FT} - k(z)}{\tau_{FT}}, \text{with } k(z) = \begin{cases} 1, & \text{if } z \geq z_i \\ 0, & \text{otherwise} \end{cases} \tag{3.6}$$

Where τ_{FT} and τ_{BL} are the relaxation time scales, τ_{FT} is determined by PBL eddy turnover time τ. The largest eddies typically extend from the top to the bottom of these layers. τ can be estimated as $\tau = z_i/w^*$, where w^* is the Deardorff convective velocity scale.

It is trivial to see if the relaxation time scale is set too large. The relaxation module results in a well-mixed scalar field. If set too small, the profile will be set to its original value at each time. As a result, an appropriate relaxation time scale is critical to this approach, which means detailed sensitivity tests should be performed to determine this value, for The Second Dynamics and Chemistry of Marine Stratocumulus field study (DYCOMS-II) case [Davini et al., 2017] did a thorough test to determine this value and found that τ_{FT} larger than 4 τ will result in a well mixed scalar in PBL, and τ_{BL} larger than 0.5 τ is a

good choice. In this study, because of the limitation of research time, the time scale used in DYCOMS-II are used. Unlike DYCOMS-II, during ASTEX the PBL height is growing almost monotonically from $\sim$ 660m to $\sim$ 2050m, which results in a monotonically growing inversion height and consequently growing eddy turnover time scale. In this sense, adaptive relaxation time scales and profile with fixed multiplier are adopted. As a result, τ_{BL}, τ_{FT} and $k(z)$ are updated accordingly at each time step.

To implement the relaxation mechanism to the scalars, we make use of the first order discretization.

$$S_{BL}(t+\Delta t,z) = \frac{\Delta t}{\tau_{BL}}(\frac{z}{1000} - S_{BL}(t,z)) + S_{BL}(t,z) \tag{3.7}$$

$$S_{FT}(t+\Delta t,z) = \frac{\Delta t}{\tau_{FT}}(k(z) - S_{FT}(t,z)) + S_{FT}(t,z) \tag{3.8}$$

Where Δt is the time step length. The relaxation together with the advection and diffusion are all evolution that the scalar undergo.

3.2 Sampling for coherent structures

For 'lagging' effect detailed in Appendix B, the octant analysis designed in this research cannot be applied to the decoupling stage. Alternatively, we only use S_{BL} to do a the quadrant analysis to capture plume properties.

Figure 3.2 shows the cross-section quadrants captured at the beginning of hour 19, 5 updrafts and 1 downdraft are labeled with numbers. The lowest level with liquid water content corresponds to z_{LC} in Figure 4.1. Updraft ① and ② both reaches the inversion height with little interactions with each other. On the contrary, updraft ③ and ④ stop ascending and detrain above few levels of z_{LC}. Because of the periodic boundary conditions,

the leftmost ⑤ updraft is actually the same updraft as the rightmost updraft and also losea a large portion of its area when reaching the cloud layer. Only downdraft ⑥ is shown, and it continues to descend until reaching z_{LC}, which is consistent with the diagram shows in Figure 4.1.

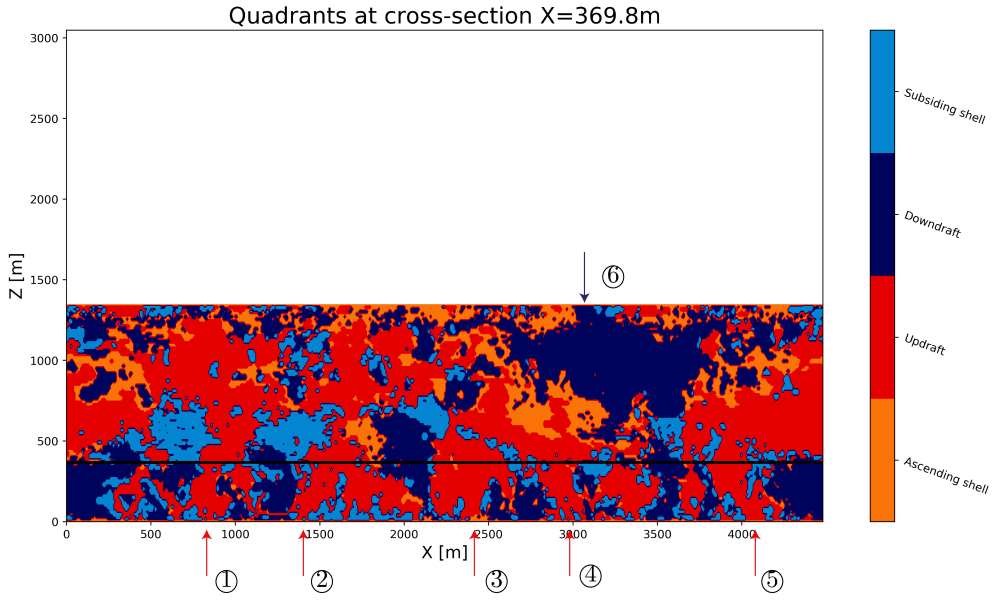

Figure 3.2: Cross-section quadrants at the beginning of hour 19 before wPDF filtering, the red arrows indicate where the updraft originate, blue arrow indicates where the downdraft originate, the lowest level with liquid content is shown with solid black line.

Figure 3.4 shows the quadrants at different heights. At the height near the surface (0.1^*z_i), updrafts are surrounded by descending shells indicating that some updraft with very weak vertical velocity has already stopped ascending and detrain. These downdrafts do not originate from free troposphere but only complement of updraft's detrainment that showing a high correlation with the descending shell. At the height near the cloud base (0.8^*z_i) the downdraft driven by radiative cooling consists of large continue area, while the updraft at this part has the ascending shell surrounded, which indicates transformations from the ascending shell to complementary updraft. Figure 3.6 shows the dynamic transformation among quadrants.

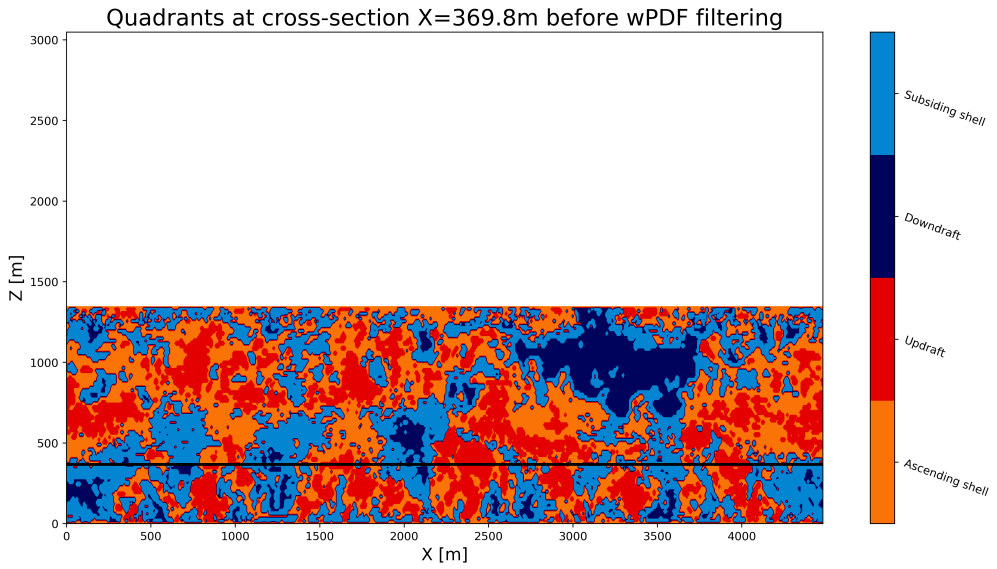

Figure 3.3: Cross-section quadrants at the beginning of hour 19 after wPDF filtering.

Figure 3.7 shows fluctuation of vertical velocity, water content and temperature within quadrants with upper and lower limits of the standard deviation (STD). The large STD indicates properties within original updraft/downdraft quadrant are diverged, which urge us to further filter out the passive plumes (PP) tha falls into the small scale turbulent shell category, and the active large scale plumes (AP). As indicated in Figure 3.6, the difference between the (AP) and (PP) roots in the velocity magnitude. Due to its small scale characteristics, (PP) is in a dynamic circle ongoing mutual transformation with the ascending/descending shells. As a result, they can't be accelerated/decelerated to a comparable vertical velocity and be considered as AP. In Figure 3.7 the vertical velocity has already shown a clear separation between the large scale coherent part and small scale turbulent part. For profiles of q_t and θ_l, the downdraft (updraft) and ascending (descending) shell show strong correlation, indicating part of the updraft/downdraft is in the dynamic cycle. To further separate the small and large scale motions within updraft and downdraft, vertical velocity probability density function (wPDF) filter is used to filter out the small

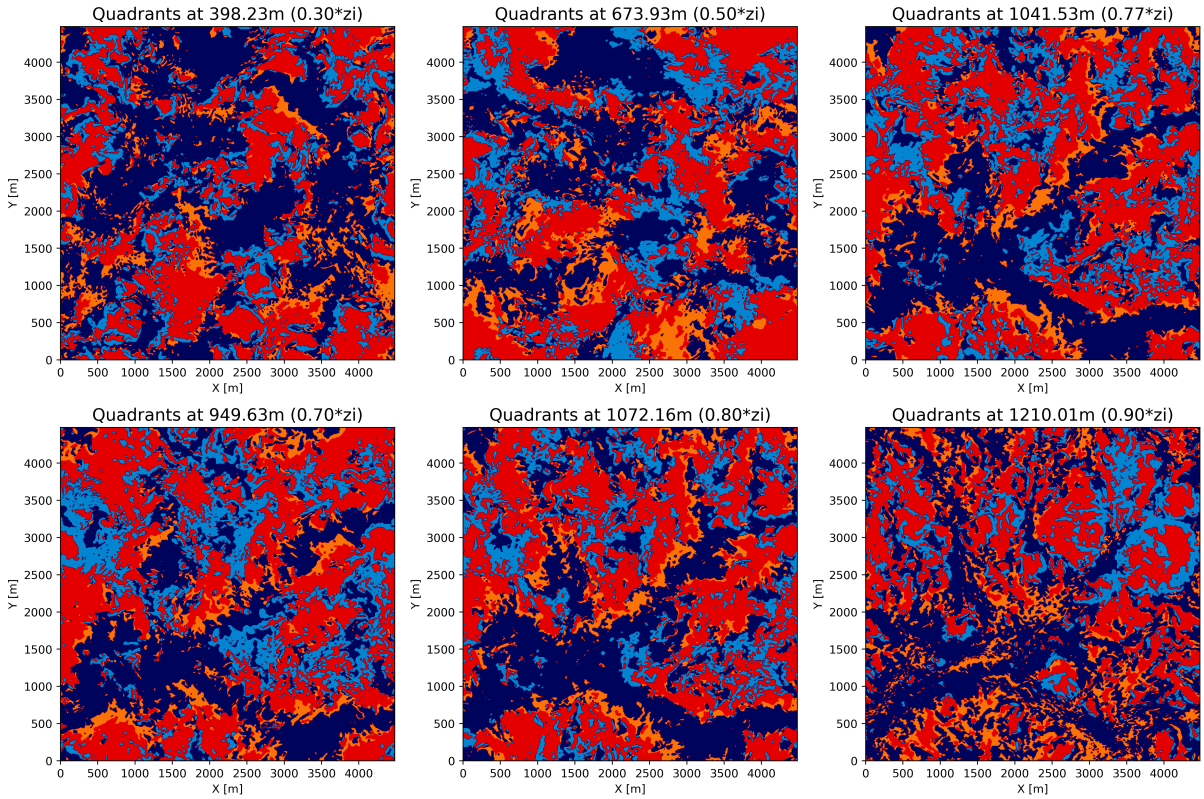

Figure 3.4: Slab quadrants at different height before using wPDF filter, colormap is the same as in Figure 3.2. (**Decoupling stage**)

scale complementary updraft/downdraft. As a result, the whole PBL is separated to six parts and the procedure is defined as "sextant" analysis, but for clarity the complementary updrafts/downdrafts are categorized as ascending/descending shell. In this research, the wPDF is chosen to be the upper/lower 10% to separate the AP and PP.

Figure 3.8 shows the final sampling approach proposed. With the primary quadrant analysis we observed a clear pattern between the 'paired' quadrants in Figure 3.7, with a clear similarity between the updraft(downdraft) and subsiding (ascending) shell and large STD within quadrants in mind, we proposed a dynamic cycle among 4 different TS. Unlike CS, TS have rather small length scales, which make them prone to changing their vertical direction by the background turbulence. In this sense, wPDF filtering is further applied to updrafts and downdrafts to further separate the AP and PP. With the two approaches

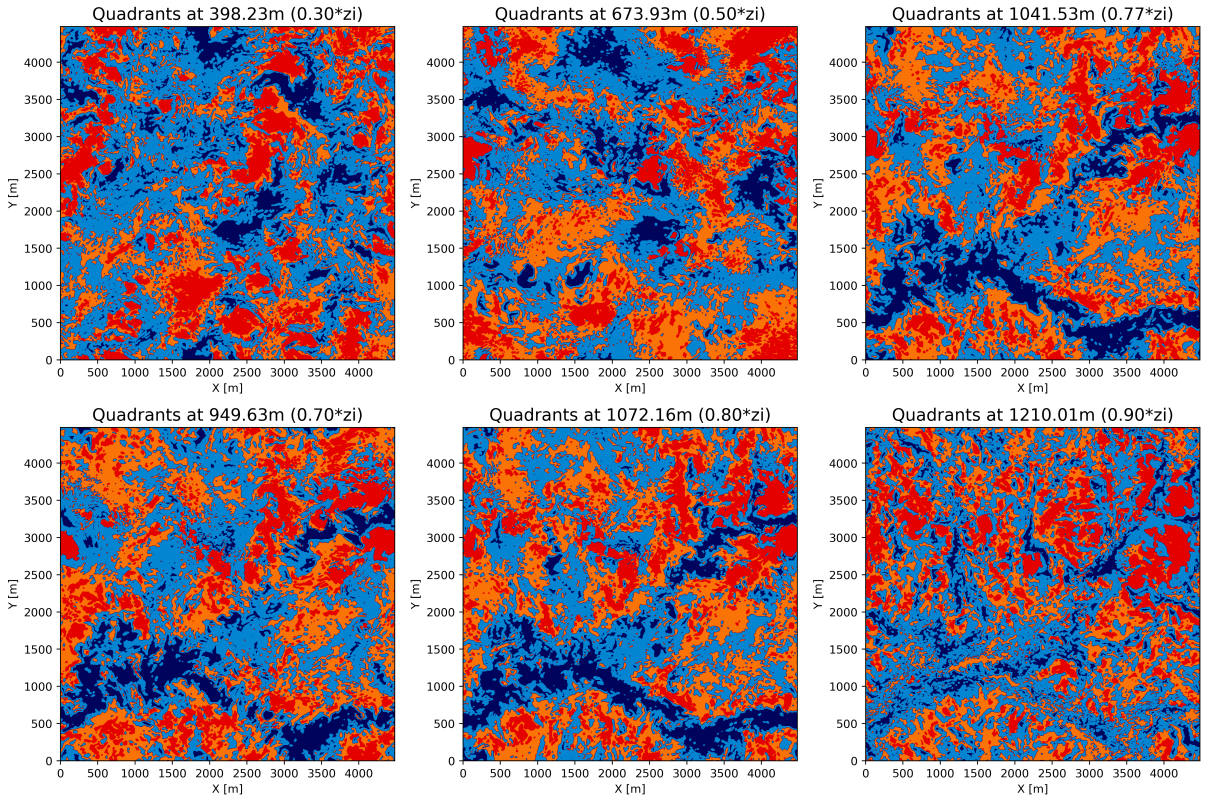

Figure 3.5: Slab quadrants at different height after using wPDF filter, colormap is the same as in Figure 3.2. (**Decoupling stage**)

combined together, the downdraft PP found in the original quadrants at surface layer goes to the subsiding shell while downdraft AP in the Sc layer was kept.

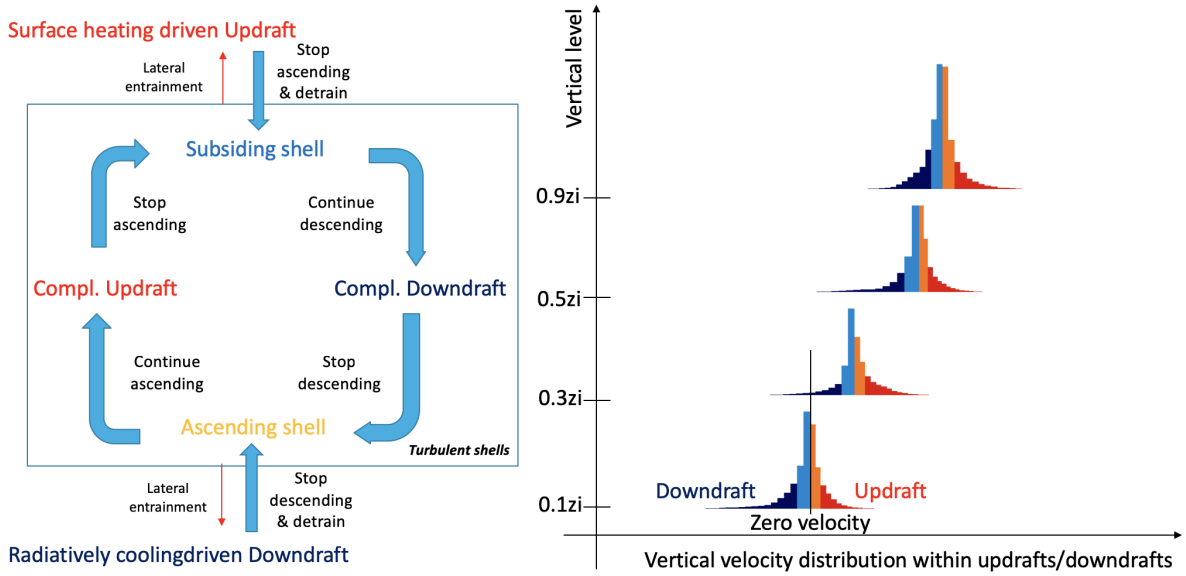

Figure 3.6: Diagram of dynamic interaction between turbulent shells and coherent structures (left) and the diagram showing the wPDF filtering approach (right).

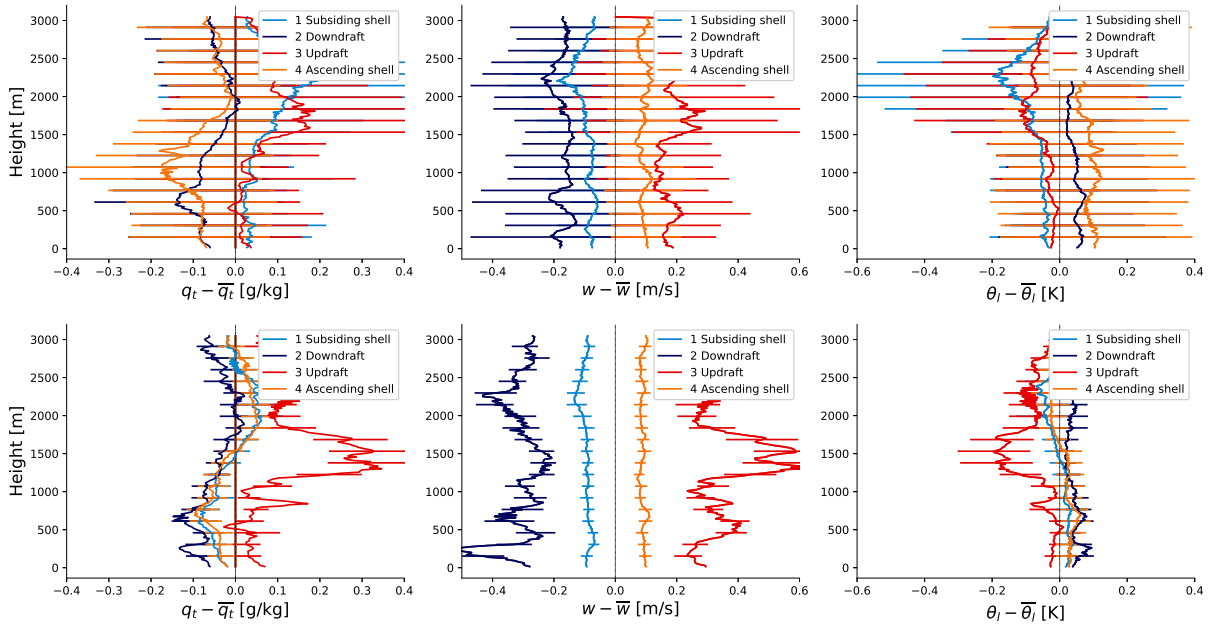

Figure 3.7: Profile of quadrant properties with error bar showing the standard deviation before (top), and after wPDF filtering (bottom).

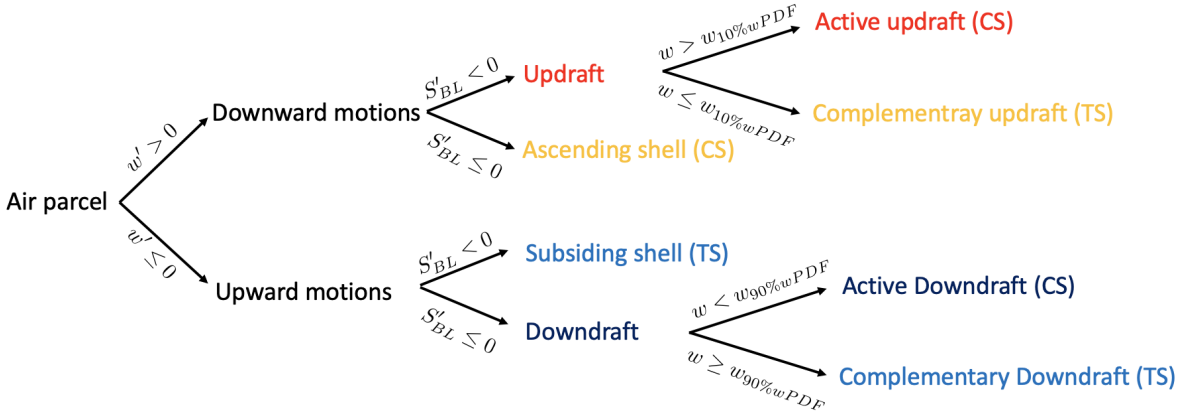

Figure 3.8: Sextant analysis using S'_{BL}, w' and wPDF criteria.

Chapter 4

Parameterization implications - dual stochastic parameterization

4.1 Variables and basic theory

Governed by a set of complex interrelated phenomenon like surface and top-down (caused by longwave cooling) convection, wind shear, drizzle, and the entrainment of free atmospheric air into the boundary layer, cumulus and stratocumulus are the most prevalent cloud types in the planetary boundary layer. The moisture and heat transport are the two major concerns in the study of atmosphere. Because of the limited computational power and the multi-scale nature of the planetary boundary layer, much of the transport has to be parameterized. Only a small portion of eddies can be resolved in NWP. In this section, the modeled transport equations need to be parameterized are described.

4.1.1 Scale in LES model and NWP model

Varing physical phenomenon coexist in the atmosphere on many magnitudes, including tropical atmospheric circulations ($\propto$ 1000km), mesoscale convective systems ($\propto$

100km), boundary layer convection and large eddies anomaly ($\propto$ 1000km) and small scale eddies beyond Kolmogorov dissipation scale (less than 1mm). Obviously, with state-of-art computation resources, one single model cannot resolve all physical process.

4.1.2 Basic theory

Atmospheric science often uses variables that are conserved for pressure change and moisture process (condensation/evaporation). The budget equation can be expressed as follows:

$$\frac{\partial \phi}{\partial t} + u_j \frac{\partial \phi}{\partial x_j} = F_\phi \tag{4.1}$$

The first term in the right hand side is the tendency of the conserved variables, u_j is velocity in j direction, F_ϕ is the sink/source term posted by another physical process, such as surface moisture/heat flux or the rain water condensation, ϕ is the conserved variables such as total water mixing ratio $q_t = q_l + q_v + q_i$, which correspond to the liquid water mixing ratio indicated saturated air parcel, q_v is vapor water mixing ratio, q_i is the ice water mixing ratio which is not considered in this research. The liquid water potential temperature simplifies calculations on heat transport because it is conserved for vertical movement with hydrostatic pressure change and moisture process, which can be calculated as:

$$\theta_l \approx \theta - \frac{L_v}{c_{pd}} q_l \tag{4.2}$$

Where θ is potential temperature calculated as $\theta = T\left(\frac{p_0}{p}\right)^\kappa$,$\kappa$ is defined as the ratio of the specific gas constant of dry air R_d and the heat capacity c_{pd} and assumed 2/7, L_v the latent heat of vaporization, c_{pd} the specific heat of dry air, and q_l the liquid water mixing ratio. In the calculation of buoyancy, density should be considered with temperature. In this sense, the virtual temperature is introduced as a temperature scale which can be used

for buoyancy, which is calculated as,

$$\theta_v = \left(1 + \frac{1-\epsilon}{\epsilon} q_t - \frac{q_l}{\epsilon}\right)\left(\theta_l + \frac{L_v}{c_p} q_l\right) \tag{4.3}$$

ϵ is specific gas constant of water vapor $\epsilon = R_d/R_v \approx 0.622$. Because the density of water vapor is lighter than air, the total water mixing ratio acts as a source term for the buoyancy, whereas the liquid water act as a sink term because it is much heavier. For the second term, the liquid water also acts as a source term due to latent heat release from condensation. The lapse rate for the θ_v is an important indicator for stability in the atmosphere. With positive rate, the air parcels above are less dense and the turbulence is suppressed. When the environment lapse rate is large enough, any rising air parcel will be colder than the environment, and will sink back down and atmosphere is characterized as absolutely stable because no matter if the parcel is saturated or not, it cannot become buoyant. With negative θ_l lapse rate, air parcels are denser than lower parcels and the environment become unstable. In this research, the prognostic variable for heat is the liquid water potential temperature, for water is the total water mixing ratio, and the virtual potential temperature θ_v are used for parameterization.

4.2 Decomposition of turbulent transport

If there exists a clear separation of scales between the sub-grid eddies and grid-scale motions, the budget equation 4.1 for conserved variables $\phi \in (\theta_l, q_t)$ in the Boussinesq approximation can be read as:

$$\frac{\partial \overline{\phi}}{\partial t} = -\frac{\partial \overline{w'\phi'}}{\partial z} + F_\phi \tag{4.4}$$

The overline indicates the environmental mean. The first term on the right hand side is the lapse rate for the kinematic flux of variables, which is called turbulent transport. Eddies

with large q_t' and low θ_l'. Eddies with positive vertical velocity perturbation perform upward water and downward heat transport, and vice versa. F_ϕ term, if no adiabatic process and zero mean wind is presented, becomes zero and total tendency can be simply represented by the turbulent transport term. In the same sense, with the covariance multiplied by the vertical velocity perturbation, the turbulent transport term for other variables can be shown. Most of the difficulty is the calculation of the turbulent flux $w'\phi'$, which arises from the decomposition of the budget equation into mean quantities and turbulent fluctuations.

The EDMF parameterization in this research mainly follows [Sušelj et al., 2012, Sušelj et al., 2013], but the parameters, are diagnosed from a conditional sampling approach adapted from [Davini et al., 2017]. In addition, a comparative parameterization for downdraft is introduced. As a result, the framework of the stochastic dual EDMF parameterization is developed as follows. The updrafts are initialized with fixed fraction at the surface given the properties of surface determined by the Monin–Obukhov similarity [Stull, 1988]. Then integrate vertical velocity within the updraft following a simplified velocity budget until condensation occurs. When the condensation occurs, the updraft is split to a predefined number of updrafts, and their properties are determined stochastically from bivariate probability density function (PDF) diagnosed from LES. Because of lateral entrainment, the updrafts will decelerate until the vertical velocity approaches zero, resulting in detrainment and decrease of the updraft area. While the downdraft is initialized at the cloud base with properties draw from bivariate PDF of θ_l and q_t, integrating its vertical velocity with the same budget but the buoyancy as a sink term, the lateral entrainment is similar to the updraft but with different parameters. As a consequence, it will stop descending before it hits z_{LC} level.

A closed PBL parameterization scheme gives flux profiles within the PBL and the overlying air, providing tendencies of temperature, moisture, and horizontal momentum for the entire atmospheric column. The major difference in PBL parameterizations lies in

the modeling of turbulent flux terms. In this section, existing PBL parameterization is explained and discussed.

Pure ED parameterization formulated as in [Holtslag and Moeng, 1991] can be shown as follows,

$$\overline{w'\phi'} = -K\frac{\partial \phi}{\partial z} \tag{4.5}$$

The eddy diffusivity K is often parameterized as a function of TKE (Turbulent kinetic energy, calculated as $\frac{1}{2}\left(\overline{u'^2}+\overline{v'^2}+\overline{w'^2}\right)$), and a turbulence mixing length scale L_m and a stability correction function differs for heat and momentum. Section 4.4 will give a detailed discussion about the parameterization of K.

As mentioned in section 5, a major part of turbulent transport is fulfilled by strong organized coherent structures. For the updraft/downdraft/environment separation, the decomposition can be expressed as follows,

$$\overline{w'\phi'} \approx \underbrace{a_u(w_u-\overline{w})}_{M_u}(\phi_u-\overline{\phi}) + \underbrace{a_d(w_d-\overline{w})}_{M_d}(\phi_d-\overline{\phi}) + (1-a_u-a_d)(w_{env}-\overline{w})(\phi_{env}-\overline{\phi}) \tag{4.6}$$

Where a_u and a_d are area fractions for the downdraft and updraft, w the vertical velocity, M_u and M_d are mass flux of the thermal, the residue term in the right hand side is often parameterized as the small scale passive environmental local mixing through eddy diffusion approach.

$$\overline{w'\phi'_{env}} = (1-a_u-a_d)(w_{env}-\overline{w})(\phi_{env}-\overline{\phi}) \approx -K_\phi\frac{\partial \overline{\phi}}{\partial z} \tag{4.7}$$

Together with equation 4.6, the final form for the state-of-art EDMF parameterization assuming multiple updrafts:

$$\overline{w'\phi'} = -K_\phi(z)\,\frac{\partial \overline{\phi}}{\partial z} + \sum_{i=1}^{n} M_{u,i}(\phi_{u,i}-\overline{\phi}) + \sum_{i=1}^{n} M_{d,i}(\phi_{d,i}-\overline{\phi}) \tag{4.8}$$

Above formula effectively separate the "non-local" or counter gradient MF part and the

local mixing part by eddy diffusion approach and is the start of the EDMF parameterization proposed in this research. Though explicitly expressed in equation 4.6, current EDMF schemes typically only consider updrafts and model the downdraft into the eddy diffusion part. It holds for some situations such as clear convective and shallow cumulus boundary layers [Handa, 2018], where downdrafts are produced by the mass conservation as a consequence of surface heat-driven thermal updrafts.

4.3 Mass-flux parameterization

4.3.1 Original scheme revisit

The budget equation for prognostic variables within the downdraft/updraft:

$$\frac{\partial \phi_p}{\partial z} = -\epsilon(\phi_p - \overline{\phi}) + F_\phi \text{ where, } \phi = (\theta_l,\ q_t) \tag{4.9}$$

The left hand side is the lapse rate of the variables within coherent structures. Subscript p for there and in the following represents the plumes (updrafts and downdrafts). ϵ is lateral entrainment rate determined by a stochastic approach, which is described in the following section. F_ϕ contains source/sink terms due to the interaction with the environment, except the lateral entrainment. It is assumed that except the lateral entrainment, no other physical interactions with the environment and all the entrained air have the same properties as the environment where the entrainment happens, so F_ϕ here is assumed as zero.

Updraft initialization

Following the arrangement in [Sušelj et al., 2012], the dry updrafts are initialized at the surface:

$$w_u|s = \alpha_w w_* \tag{4.10}$$

$$\theta_{lu}|s = \theta_l|s + \alpha_{\theta_l}\frac{\overline{w'\theta_l'}|s}{w_*} \tag{4.11}$$

$$q_{tu}|s = q_t|s + \alpha_{q_t}\frac{\overline{w'q_t'}|s}{w_*} \tag{4.12}$$

where $\alpha_{\theta_l} = \alpha_{q_t} = 1.4$, $\alpha_w = 0.8$, w_* is Deardorff convective velocity scale [Deardorff, 1970]. calculated as $w^* = \left[\frac{g}{T_v} z_i \left.\overline{w'\theta_v'}\right|_s\right]^{\frac{1}{3}}$, where $g = 9.8m/s^2$ is gravity acceleration, T_v is absolute temperature, the $\left.\overline{w'\theta_v'}\right|_s$ term denotes the surface kinematic vertical turbulent flux of buoyancy. z_i is boundary layer height, which can be determined by minimum flux/gradient in some scalar or monitoring a threshold value of some scalar, such as liquid water virtual temperature θ_v, liquid water mixing ratio q_l and liquid water potential temperature θ_l. In this study, the gradient of θ_v is used to determine z_i. $\overline{w'\theta_l'}/\overline{w'q_t'}$ is surface sensible/latent heat flux, which is directly or indirectly set as boundary condition.

Lateral entrainment

The lateral entrainment for updraft is designed to be a stochastic process following [Sušelj et al., 2013]:

$$\epsilon(\Delta z) = \frac{1}{\Delta z}\epsilon_d \frac{\Delta z}{L_0} e^{-\frac{\Delta z}{L_0}} \tag{4.13}$$

Δz is the vertical displacement of downdraft/updraft, $\epsilon = 0.1$ denotes each entrainment event entrains 10% of the mass flux of the updraft/downdraft. The probability part $\frac{\Delta z}{L_0} e^{-\frac{\Delta z}{L_0}}$ resembles a Poisson distribution ($P(k\ events\ in\ interval) = e^{\lambda}\frac{(\lambda)^k}{k!}$), where the $k = 1$ and the event rate $\lambda = \frac{\Delta z}{L_0}$, which denotes on average with specified distance interval L_0 the length the updrafts/downdrafts need to ascend/descend Δz to fulfill a condensation/evaporation process. L_0 is calculated as $L_0 = \frac{z_i - z_{LC}}{10}$, where z_{LC} is level of condensation of air parcel within the updraft/downdraft.

Vertical integration

Vertical velocity budget can be divided to the following parts [de Roode et al., 2012]:

$$\underbrace{\frac{\partial w_p}{\partial t}}_{\text{Tend}} = \underbrace{\frac{g}{\theta_0}(\theta_{v,c} - \overline{\theta_v})}_{\text{Buo}} - \underbrace{\frac{1}{2}\frac{\partial w_p^2}{\partial z}}_{\text{Adv}} - \underbrace{\frac{\epsilon_w w_p^2}{1-\sigma_p}}_{\text{entr}} - \underbrace{\frac{1}{\sigma_p}\frac{\partial a_p \overline{w'' w''^u}}{\partial z}}_{\text{Subplume}} - \underbrace{\left[\frac{\partial p}{\partial z}\right]_c}_{\text{Pres}} + \underbrace{2\Omega \cos\phi_l \sigma_p u_p}_{\text{Cor}} \tag{4.14}$$

In equation 4.14, the subscript p denotes the downdrafts/updrafts within PBL. On the right hand side, the buoyancy term (buo) is the main source term, while entrainment (entr) terms are main sink terms for the vertical velocity. The vertical velocity within coherent structure changes in time but often steady state situation is assumed, so the left hand side vanishes and this budget equation can be further simplified with fixed updraft fraction:

$$\frac{1}{2}\frac{\partial w_p^2}{\partial z} = a\frac{g}{\theta_0}(\theta_{v,p} - \overline{\theta_v}) - (b + c\epsilon)w_p^2 \tag{4.15}$$

where $a = 2/3$, $b = 0.002m^{-1}$, and $c = 1.5$ in [Sušelj et al., 2012]. The effects of pressure perturbation and subplume can be taken into account by introducing the a, b, c term to the buoyancy term and lateral entrainment term.

Condensation

$$N = 0.5 + 0.36\arctan(1.55Q) \tag{4.16}$$

$$q_l = \sigma_s \begin{cases} e^{(1.2Q-1)} & Q < 0 \\ e^{-1} + 0.66Q + 0.086Q^2 & Q \geq 0 \end{cases} \tag{4.17}$$

[Cuijpers and P.BECHTOLD, 1995] Where N is a portion of the moist updraft or the partial cloudiness, Q is the ratio of saturation deficit s and its standard deviation σ_s: $Q = s/\sigma_s$. For $Q \geq 0$ (stratocumulus cloud), the Gaussian distribution is well satisfied,

while $Q < 0$ (trade-wind cumulus) is characterized by a positively skewed distribution function. Equation 4.17 linearly interpolated between the Gaussian distribution and a distribution with known positive skewness to fit the Sc and Cu regime. Using Equation 4.16, cloudiness scheme is coupled with turbulence scheme(cloudiness-turbulence scheme). The key part to simulate the Sc-Cu transition is correct representation of the Sc Gaussian distribution and Cu positive skewness distribution. s measures the saturation excess $s = q_t - q_s$, using truncated Taylor expansion for $q_s(T)$ around T_l by:

$$q_s(T) = q_s(T_l) + \frac{\partial q_s}{\partial T}|_{(T=T_l)}(T - T_l) \tag{4.18}$$

Substitute $T_l/T = \theta_l/\theta$ and $T_l = Lq_l/c_p$, where L_v is latent heat of vaporization of water, with $\theta_l = \theta_l(1 - Lq_l/c_pT)$ the equation 4.18 becomes:

$$q_s(T) = q_s(T_l) + \frac{\partial q_s}{\partial T}|_{(T=T_l)}(\theta_l' T/\theta - L_v q_l/c_p) \tag{4.19}$$

And the saturation deficit follows:

$$s = aq_t' - b\theta_l' + c \tag{4.20}$$

Where $a = \frac{1}{1+\gamma}$, $b = a(T/\theta)\frac{\partial q_s}{\partial T}|_{(T=T_l)}$, $c = a(q_t - q_s(T_l))$, $\gamma = (L/c_p)/\frac{\partial q_s}{\partial T}|_{(T=T_l)}$, σ_s is variance of s and calculated as:

$$\sigma_s = (\overline{s'^2})^{1/2} = \frac{1}{2}\left[(aq_t' - b\theta_l')^2\right]^{\frac{1}{2}} = \frac{1}{2}\left[a^2\overline{q_t'q_t'} + b^2\overline{\theta_l'\theta_l'} - 2ab\overline{\theta_l'q_t'}\right]^{\frac{1}{2}} \tag{4.21}$$

Substitute the variance($\overline{\phi'\phi'} = \frac{2\tau}{C}\overline{w'\phi'}\frac{\partial\phi}{\partial z}$) and covariance estimated in [Sušelj et al., 2013]:

$$\sigma_s = \frac{a\tau_s^{1/2}}{2C_\epsilon}\left(b\overline{w'\theta_l'}\frac{\partial q_t}{\partial z} + b\overline{w'q_t'}\frac{\partial\theta_l}{\partial z} - \overline{w'q_t'}\frac{\partial q_t}{\partial z} - b^2\overline{w'\theta_l'}\frac{\partial\theta_l}{\partial z}\right)^{\frac{1}{2}} \tag{4.22}$$

Where a and b are the same as in equation 4.20, $C_\epsilon = 0.16$ and time scale $\tau_s = 0.1 z_i / w_*$.

The final closure requires the boundary conditions for both the dry updrafts and moist updrafts at the level of condensation are determined by bivariate PDF, the Gaussian distribution for q_t and θ_l can be expressed as:

$$G = \frac{1}{2\pi\sigma_{\theta_{lp}}\sigma_{q_{tp}}(1-\rho^2)^{1/2}} \times \exp\left[-\frac{1}{2(1-\rho^2)}\left\{\frac{\theta_{lp}'^2}{\sigma_{\theta_{lp}}^2} - 2\rho\frac{\theta_l' q_{tp}'}{\sigma_{\theta_{lp}}\sigma_{q_{tp}}} + \frac{q_{tp}'^2}{\sigma_{q_{tp}}^2}\right\}\right] \tag{4.23}$$

Where $\sigma_{\theta_{lc}} \equiv \theta_{lc}'^2$, $\sigma_{q_{tc}} \equiv q_{tc}'^2$, $\rho \equiv \mathrm{cov}(q_{tc}, \theta_{lc}) = \frac{\overline{\theta_{lc}' q_{tc}'}}{\sigma_{\theta_{lc}}\sigma_{q_{tc}}}$. Using the variance/covariance estimated in [Sušelj et al., 2013]:

$$\overline{\phi_p' \phi_p'} = \frac{3}{2}\frac{\tau_p^2}{C} w_p^2 \epsilon^2 (\phi_p - \phi)^2 \tag{4.24}$$

$$\overline{w_p' w_p'} = \frac{1}{2} w_p^2, \tag{4.25}$$

$$\overline{q_{tp}' w_p'} = 0, \tag{4.26}$$

$$\overline{\theta_{lp}' w_p'} = 0.6(\overline{\theta_{lp}' \theta_{lp}'} \times \overline{q_{tp}' q_{tp}'})^{1/2} \tag{4.27}$$

$$\overline{\theta_{lp}' q_t'} = 0.7(\overline{\theta_{lp}' \theta_{lp}'} \times \overline{q_{tp}' q_{tp}'})^{1/2} \mathrm{sign}\Big[(\theta_{lp} - \theta_l)(q_{tp} - q_t)\Big] \tag{4.28}$$

Where $C = 1$ and $\tau_p = 300s$, hereafter, the mass flux parameterization for updraft is closed.

4.3.2 Two modifications

Downdrafts initialized from Sc base

With the evolution of the three-layer-structure during transition, we know clear representation of the gradually decreasing downward non-local mixing is crucial to Sc-Cu transition. With sampled downdraft at the cloud top, we propose to add a downdraft part comparable to the surface initialized updraft with similar vertical velocity and lateral

entrainment. The initial boundary condition including downdraft fraction is determined by bivariate PDF sampled at the Sc base. Because the downdraft is dry and warm, as it goes down the temperature grows warmer that inhibits condensation, set no condensation for the downdraft.

Lateral entrainment by paired TS

With the sextant analysis in Chapter 3. We know the AP are surrounded by their paired TS, which are separated by the wPDF filtering. So, unlike the original scheme of using the environment as lateral entrainment property, we proposed to use paired TS as for the air entrains into the AP.

4.4 Eddy-diffusivity parameterization

No modifications are made in the ED parametrization, the original part will be shown there for completeness.

The eddy diffusivity parameterization part follows [Sušelj et al., 2013] where K is parameterized with the square root of TKE and a mixing length:

$$K_\phi = l\sqrt{e} \tag{4.29}$$

where $l = l_{23} + (l_1 - l_{23})e^{-z/0.1z_i}$, with $l_{23}^{-1} = l_2^{-1} + l_3^{-1}$. Where $l_1 = \kappa z$ with κ the Von Karman constant, $l_2 = 400\sqrt{e}$, $l_3 = 0.7\frac{\sqrt{e}}{N}$ with $N = \sqrt{(g/\theta_v)(\partial\theta_v/\partial z)}$ the buoyancy frequency.

The budget equation for TKE:

$$\underbrace{\frac{\partial e}{\partial t}}_{storage} = \underbrace{\frac{g}{\theta_v}\overline{w'\theta_v'}}_{buoyancy} - \underbrace{(\overline{w'u'}\frac{\partial U}{\partial z} + \overline{w'v'}\frac{\partial V}{\partial z})}_{shear} - \underbrace{\frac{\partial \overline{w'e}}{\partial z}}_{transport} - \underbrace{W\frac{\partial e'}{\partial z}}_{advection} - \underbrace{\epsilon}_{dissipation} \tag{4.30}$$

where the buoyancy, transport, advection and dissipation terms are parameterized following [Sušelj et al., 2012]. The surface boundary condition is imposed with formula $e|_s = 7.5u_*^2 + 0.4w_*^2$, where u_* is surface friction velocity $u_* = \left[(\overline{u'w'})^2 + (\overline{v'w'})^2\right]^{1/4}$ and w_* is Deardorff convective velocity scale calculates as in equation 4.12.

The 'stochastic' characteristics of this parameterization root in the following parts:

- Lateral entrainment is set as a stochastic process with the probability of entrainment decided by Poisson distribution with event rate as ratio of the vertical displacement and the distance that plumes need to travel before experiencing one condensation process.
- The boundary condition after the condensation is connected with a empirical fit of the bivariate PDF of θ_l and q_t.
- The cloudiness (liquid water content) and q_l is determined using a empirical relation with a stochastic turbulence scheme.

However, the framework of EDMF itself maintains to be a deterministic model because:

- EDMF adapts the coherent structures and represents the turbulence transport mainly by tracing the air motion within it, which maintains the deterministic view of turbulence.
- Only the usage of bivariate PDF introduces the stochastic component, while the PDF itself can be further optimized to have more 'deterministic' sense.

In this chapter, with the state-of-art stochastic EDMF parameterization as a base model. We proposed two major modifications based on findings from the three-layer-structure in LES results and sextant analysis. A new scheme is shown in Figure 4.1, but testing it is beyond our research goal and maybe fulfilled in the future.

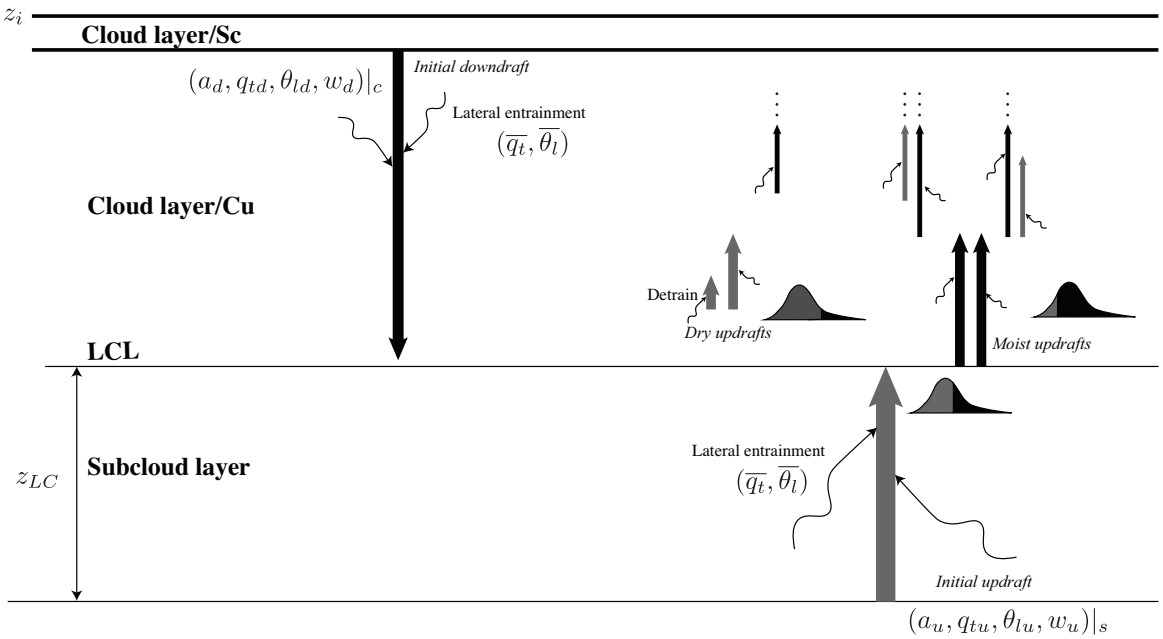

Figure 4.1: Diagram showing the stochastic mass flux scheme. Black arrows indicate updraft/downdraft, gray arrow is dry updrafts, length of arrow shows the magnitude of vertical velocity, z_{LC} is where the saturation begin to happen.

Chapter 5

Discussion and conclusion

5.1 Conclusion

A clear three-layer-structure can be observed during the decoupling stage by looking at the vertical profiles of the conserved variables: i) a well-mixed surface layer driven by surface heating; ii) a cumulus layer with the sources of heating and moisture feeding from the surface and cooling & drying from stratocumulus layer but without sufficient TKE to mixe them together; iii) a well-mixed stratocumulus layer driven by radiative cooling. During the decoupling stage, Sc layer is constantly thinned due to the insufficient moisture feeding from the surface layer, which results in a constantly decreasing downward turbulent mixing and further decoupling. Finally, the Sc layer is fully dissolved, leaving only the Cu layer. The LES study of ASTEX shows that the clear representation of the downward non-local mixing within the Sc layer might be a crucial part in the representation of the Sc-Cu transition in the large scale models.

Quadrant analysis shows that there exists a dynamic cycle within turbulent shells: i) complementary updraft/downdraft transferred from ascending/descending shell that continues to ascend/descend; ii) the ascending/descending shell itself can be transferred

from updraft/downdraft stops ascending/descending. Based on the constantly changing vertical direction of the turbulent shells, a sextant analysis with wPDF filtering is used to further separate the complementary and driven parts.

With the sampled plume properties and the detailed sextant analysis. Two major modifications were made on the state-of-art stochastic EDMF parameterization: i) a comparable downdraft initialized from stratocumulus cloud base is added to account for the gradually decreasing downward mixing driven by radiative cooling during Sc-Cu transition; ii) properties within the paired turbulent shell for updraft/downdraft are used to fulfill the later entrainment, rather than the environment in the original form.

5.2 Future research

- The time scale, which controls the relaxation of the S_{FT}, needs more detailed sensitivity tests. Because unlike [Davini et al., 2017], the inversion height in the ASTEX case is growing and consequently leaves an additional time scale that should be considered. Together with the eddy turnover time scale, a more complex time scale commands further study. With several tests not include here, the proper value for τ_{FT} would be much smaller than the original 4τ and should be even smaller as the PBL depth grows. It may approach near 0.5τ, but then it loses its physical meaning. An alternative approach is to perform several steady state transition simulations as [Chung et al., 2012] with a fixed depth of PBL to eliminate the effects of the changing PBL height. However, in present research, using fixed ratio $\tau_{FT} = 4\tau$ resulted in two stratified boundary layers after 4 hours, which is non-physical and cannot be used further after that time point for octant analysis. An alternative approach with existing LES results is mentioned in Appendix B.

- Some additional passive scalars like [Brient et al., 2019] may help to validate the

sextant analysis in this research. Also, the relaxation time scales in this research can be calculated with other length scale such as the diameter of the active plumes to fit the definition of "eddy turnover time" more precisely.

- To implement the dual stochastic parameterization proposed in this research with NWP mode, several test in the single column model (SCM) are necessary; a steady ASTEX like [Chung et al., 2012] is a good start.

Appendix A

Quadrants at stratocumulus stage and cumulus stage

In this appendix, quadrants captured for the stratocumulus and cumulus stage at the same slice as Figure 3.5 are shown.

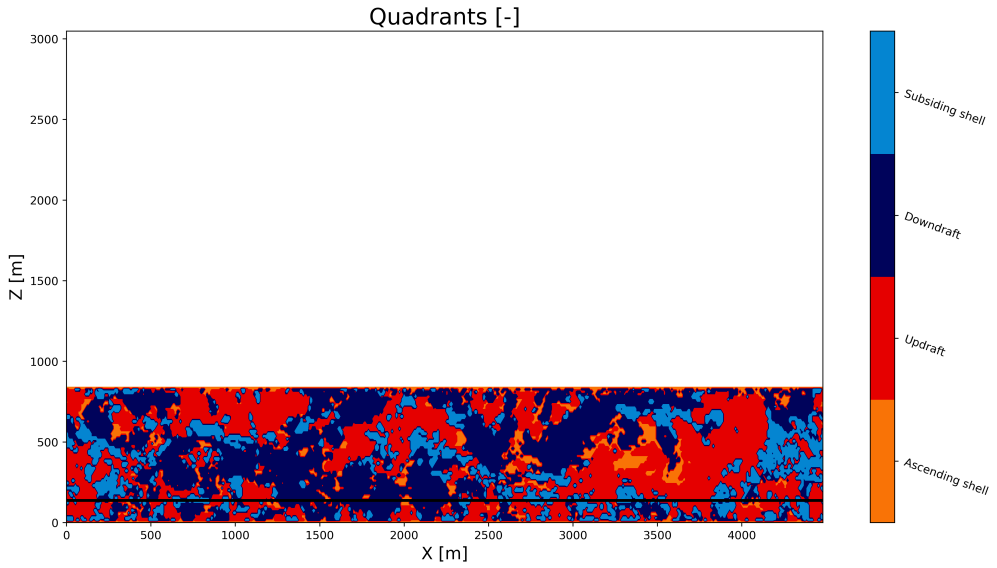

Figure A.1: Cross section quadrants at the beginning of hour 4. (**Stratocumulus stage**)

.

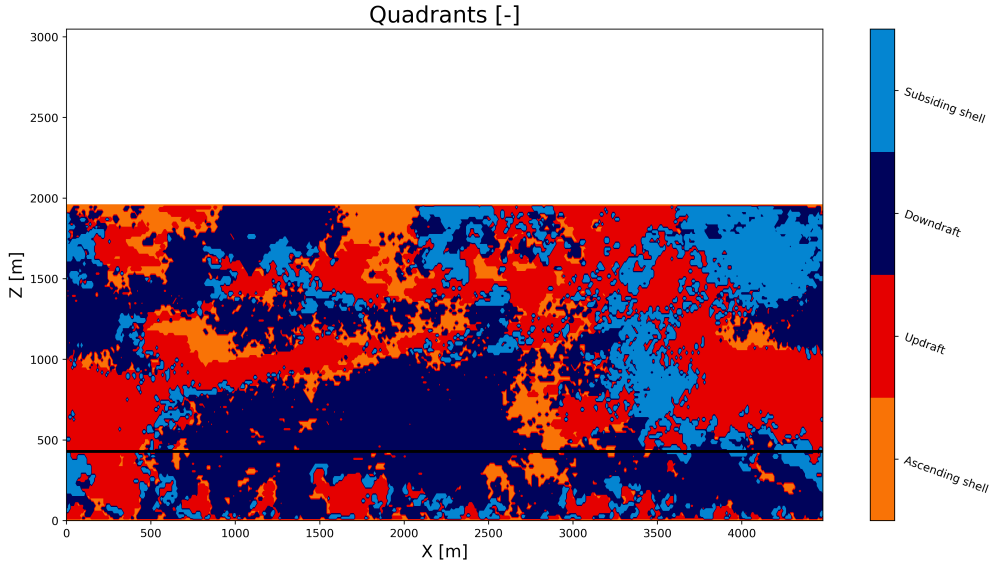

Figure A.2: Cross section quadrants at the beginning of hour 38. (**Cumulus stage**)

.

Appendix B

Discussion about octants

As shown in Figure 2.10, the S_{FT} shows a clear two layer structure. Therefore performing the same octant analysis in [Davini et al., 2017] is impossible. It is trivial to see that there will be too much downward PBL plumes considered as entrainment. Consequently, other plumes will be incorrectly considered as air motion from the free troposphere. The reason is rooted in the inappropriate manipulation of S_{FT} in the ASTEX case. The inversion height is monotonically growing and the growing rate introduces an additional time scale that needs to be addressed or there will be 'lagging' effects after updating the relaxation profile. For example, imagine you have a cup of water with coffee powder on the top of it. If you do nothing the coffee content will entrain the water and give you a clear indicator for entrainment related event. However, for the ASTEX case, it is like you are adding water from the bottom (PBL height growing). Although large portions of the coffee power will go up with the water (update the relaxation profile), some of it will stick to the inner wall of the cup (time lag due to incorrect relaxation time scale), creating a local maximum concentration and promoting local mixing with water above and below. If the water is added fast enough, all the water above the initial inversion height will show a degree of mixing with the coffee (free troposphere), and invalidate the tracer.

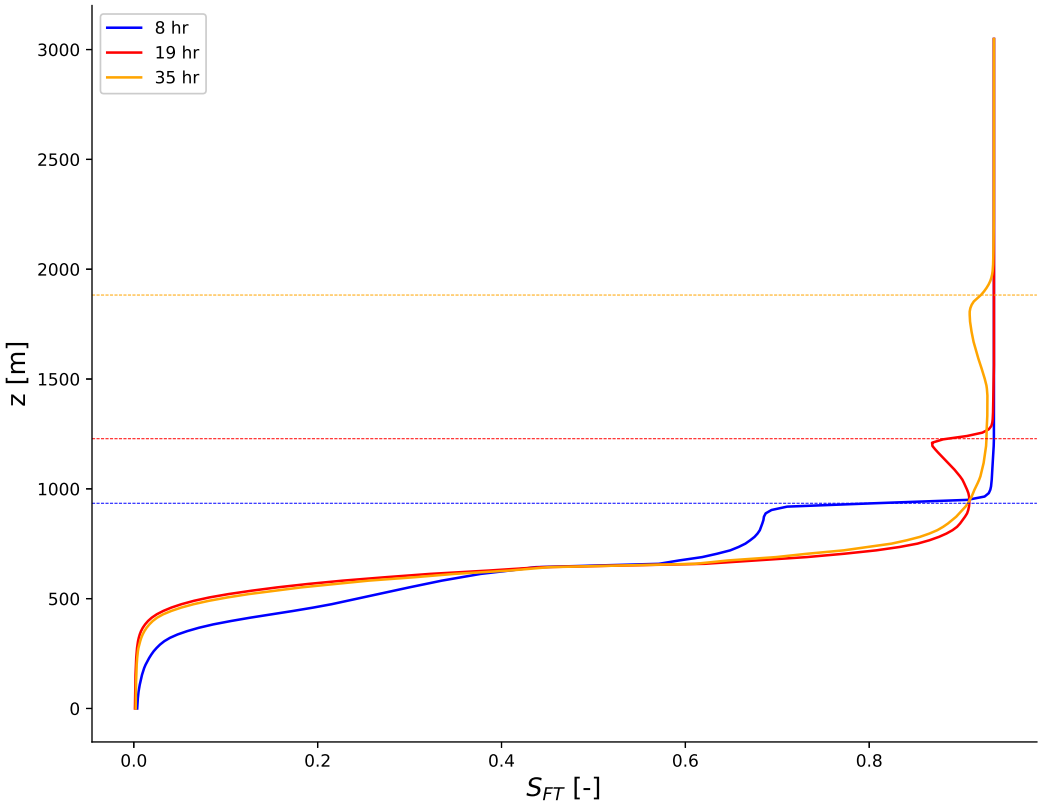

Figure B.1: Slab-average profile for S_{FT} at the beginning of hour 8, 19 and 36, corresponding inversion height is shown with dashed lines.

The key to draw an alternative way of performing the octant analysis based on existing LES is to identify the concentration of S_{FT} due to the local mixing and tropospheric motion. Figure B.1 shows the slab-average profile of S_{FT} at the observation time point. A "minimum entrainment height" can be defined as a height that the gradient of S_{FT} is zero where "local" mixing meets the mixing due to entrainment-related events. With that we can do a 'local' octant analysis only above the "minimum entrainment height".

Appendix C

Modified DALES model

Code structure and modifications for DALES 4.2 are shown in Figure C.1. Red colored codes are modified, gray colored codes are not used during simulation, and green colored codes are new codes that were introduced. The new routines read the initial profile of the decaying scalars in plain text form with *sc.inp*. The decaying scalars, together with other scalars including the velocity and thermodynamic values are initialized with *modstarup.f90*. After that, all the large scale forcing and surface fluxes are read from *modtimedep.f90*. The *modtimedepsc.f90* is called in the initialization stage, reads the surface flux and large scale forcing for the additional scalars. *modrelax.f90* is called after diagnosis modules and before the field dump module to update the new τ_{FT}, τ_{BL} and relax the decaying scalar to a designated value.

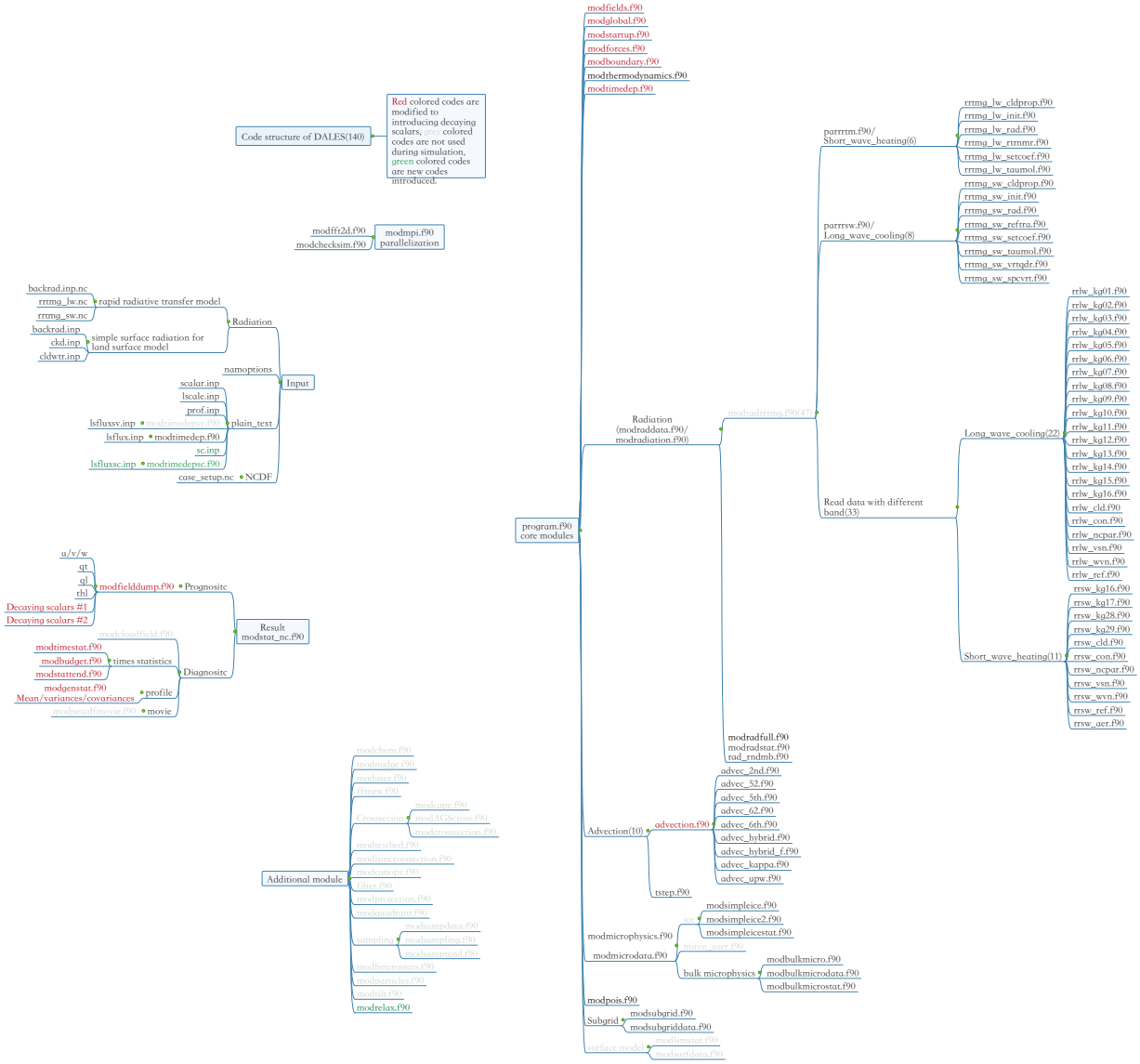

Figure C.1: Code structure and modifications for DALES 4.2.

Bibliography

[Albrecht et al., 1995] Albrecht, B. A., Bretherton, C., Johnson, D., Scubert, W. H., and Frisch, A. S. (1995). The Atlantic Stratocumulus Transition Experiment - ASTEX. *Bulletin of the American Meteorological Society*, 76(6):889–904.

[Bechtold et al., 1995] Bechtold, P., Cuijpers, J. W. M., Mascart, P., and Trouilhet, P. (1995). Modeling of Trade Wind Cumuli with a Low-Order Turbulence Model: Toward a Unified Description of Cu and Se Clouds in Meteorological Models.

[Berg and Stull, 2004] Berg, L. K. and Stull, R. B. (2004). Parameterization of Joint Frequency Distributions of Potential Temperature and Water Vapor Mixing Ratio in the Daytime Convective Boundary Layer. *Journal of the Atmospheric Sciences*, 61(7):813–828.

[Bretherton and Wyant, 1997] Bretherton, C. S. and Wyant, M. C. (1997). Moisture Transport, Lower-Tropospheric Stability, and Decoupling of Cloud-Topped Boundary Layers. *Journal of the Atmospheric Sciences*, 54(1):148–167.

[Brient et al., 2019] Brient, F., Couvreux, F., Villefranque, N., Rio, C., and Honnert, R. (2019). Object-oriented identification of coherent structures in large-eddy simulations : Importance of downdrafts in stratocumulus.

[Chandra et al., 2010] Chandra, A. S., Kollias, P., Giangrande, S. E., and Klein, S. A. (2010). Long-term observations of the convective boundary layer using insect radar returns at the SGP ARM climate research facility. *Journal of Climate*, 23(21):5699–5714.

[Chung et al., 2012] Chung, D., Matheou, G., and Teixeira, J. (2012). Steady-State Large-Eddy Simulations to Study the Stratocumulus to Shallow Cumulus Cloud Transition. *Journal of the Atmospheric Sciences*, 69(11):3264–3276.

[Couvreux et al., 2010] Couvreux, F., Hourdin, F., and Rio, C. (2010). Resolved versus parametrized boundary-layer plumes. Part I: A parametrization-oriented conditional sampling in large-eddy simulations. *Boundary-Layer Meteorology*, 134(3):441–458.

[Cuijpers and P.BECHTOLD, 1995] Cuijpers, J. W. M. and P.BECHTOLD (1995). A simple parameterization of cloud water related variables for use in boundary layer models.

[Davini et al., 2017] Davini, P., D'Andrea, F., Park, S.-B., and Gentine, P. (2017). Coherent Structures in Large-Eddy Simulations of a Nonprecipitating Stratocumulus-Topped Boundary Layer. *Journal of the Atmospheric Sciences*, 74(12):4117–4137.

[de Roode et al., 2012] de Roode, S. R., Siebesma, A. P., Jonker, H. J. J., and de Voogd, Y. (2012). Parameterization of the Vertical Velocity Equation for Shallow Cumulus Clouds. *Monthly Weather Review*, 140(8):2424–2436.

[Deardorff, 1970] Deardorff, J. W. (1970). Convective velocity and temperature scales for the unstable planetary boundary layer and for rayleigh convection. *Journal of the Atmospheric Sciences*, 27(8):1211–1213.

[Deardorff, 1980] Deardorff, J. W. (1980). Stratocumulus-capped mixed layers derived from a three-dimensional model. *Boundary-Layer Meteorology*, 18(4):495–527.

[Fu and Liou, 1993] Fu, Q. and Liou, K. N. (1993). Parameterization of the Radiative Properties of Cirrus Clouds.

[Greenhut and Khalsa, 1982] Greenhut, G. K. and Khalsa, S. J. S. (1982). Updraft and downdraft events in the atmospheric boundary layer over the equatorial pacific ocean.

[Handa, 2018] Handa, Y. (2018). *Physical modeling of stratocumulus cloud mixing processes in numerical weather prediction models*. PhD thesis, University of California San Diego.

[Heus et al., 2010] Heus, T., van Heerwaarden, C. C., Jonker, H. J. J., Siebesma, A. P., Axelsen, S., van den Dries, K., Geoffroy, O., Moene, A. F., Pino, D., de Roode, S. R., and Vilà-Guerau de Arellano, J. (2010). Formulation of the Dutch Atmospheric Large-Eddy Simulation (DALES) and overview of its applications. *Geoscientific Model Development*, 3(2):415–444.

[Holtslag and Moeng, 1991] Holtslag, A. A. M. and Moeng, C.-H. (1991). Eddy Diffusivity and Countergradient Transport in the Convective Atmospheric Boundary Layer.

[Hu and Stamnes, 1993] Hu, Y. X. and Stamnes, K. (1993). An accurate parameterization of the radiative properties of water clouds suitable for use in climate models.

[Iacono et al., 2008] Iacono, M. J., Delamere, J. S., Mlawer, E. J., Shephard, M. W., Clough, S. A., and Collins, W. D. (2008). Radiative forcing by long-lived greenhouse gases: Calculations with the AER radia- tive transfer models. *Journal of Geophysical Research Atmospheres*, 113(D13103).

[Jiang and Shu, 1996] Jiang, G. S. and Shu, C. W. (1996). Efficient implementation of weighted WENO schemes. *Journal of Computational Physics*, 126(126):202–228.

[Kogan, 2013] Kogan, Y. (2013). A Cumulus Cloud Microphysics Parameterization for Cloud-Resolving Models. *Journal of the Atmospheric Sciences*, 70(5):1423–1436.

[KUANG and BRETHERTON, 2006] KUANG, Z. and BRETHERTON, C. S. (2006). A Mass-Flux Scheme View of a High-Resolution Simulation of a Transition from Shallow to Deep Cumulus Convection. *JOURNAL OF THE ATMOSPHERIC SCIENCES*, pages 1895–1909.

[Leeuwen, 2014] Leeuwen, A. V. (2014). EDMF parameterization during ASTEX.

[Neggers, 2009] Neggers, R. A. J. (2009). A Dual Mass Flux Framework for Boundary Layer Convection. Part II: Clouds. *Journal of the Atmospheric Sciences*, 66(6):1489–1506.

[Park et al., 2016] Park, S.-B., Gentine, P., Schneider, K., and Farge, M. (2016). Coherent Structures in the Boundary and Cloud Layers: Role of Updrafts, Subsiding Shells, and Environmental Subsidence. *Journal of the Atmospheric Sciences*, 73(4):1789–1814.

[Pope, 2000] Pope, S. B. (2000). Turbulent Flows. *Journal of Turbulence*, 1:771.

[ROODE and DUYNKERKE, 2004] ROODE, S. R. D. and DUYNKERKE, P. G. (2004). Large-Eddy Simulation : How Large is Large Enough ? *Journal of the Atmospheric Sciences*, pages 403–421.

[Sandu et al., 2010] Sandu, I., Stevens, B., and Pincus, R. (2010). On the transitions in marine boundary layer cloudiness. *Atmospheric Chemistry and Physics*, 10(5):2377–2391.

[Siebesma and Cuijpers, 1995] Siebesma, A. P. and Cuijpers, J. W. M. (1995). Evaluation of Parametric Assumptions for Shallow Cumulus Convection.

[Siebesma et al., 2007] Siebesma, A. P., Soares, P. M. M., and Teixeira, J. (2007). A Combined Eddy-Diffusivity Mass-Flux Approach for the Convective Boundary Layer. *Journal of the Atmospheric Sciences*, 64(4):1230–1248.

[SOARES et al., 2004] SOARES, Miranda, P. M. A., Siebesma, A. P., Teixeira, J., and Grande, C. (2004). An eddy-diffusivity / mass-flux parametrization for dry and shallow cumulus convection. 8:3365–3383.

[Stevens, 2000] Stevens, B. (2000). Cloud transitions and decoupling in shear-free stratocumulus-topped boundary layers. 27(16):2557–2560.

[Stull, 1988] Stull, R. B. (1988). *AN INTRODUCTION TO BOUNDARY LAYER METEOROLOGY*.

[Sušelj et al., 2013] Sušelj, K., Teixeira, J., and Chung, D. (2013). A Unified Model for Moist Convective Boundary Layers Based on a Stochastic Eddy-Diffusivity/Mass-Flux Parameterization. *Journal of the Atmospheric Sciences*, 70(7):1929–1953.

[Sušelj et al., 2012] Sušelj, K., Teixeira, J., and Matheou, G. (2012). Eddy Diffusivity/Mass Flux and Shallow Cumulus Boundary Layer: An Updraft PDF Multiple Mass Flux Scheme. *Journal of the Atmospheric Sciences*, 69(5):1513–1533.

[van der Dussen et al., 2013] van der Dussen, J. J., de Roode, S. R., Ackerman, A. S., Blossey, P. N., Bretherton, C. S., Kurowski, M. J., Lock, A. P., Neggers, R. A. J., Sandu, I., and Siebesma, A. P. (2013). The GASS/EUCLIPSE model intercomparison of the stratocumulus transition as observed during ASTEX: LES results. *Journal of Advances in Modeling Earth Systems*, 5(3):483–499.

[Van Der Dussen et al., 2016] Van Der Dussen, J. J., De Roode, S. R., and Siebesma, A. P. (2016). How large-scale subsidence affects stratocumulus transitions. *Atmospheric Chemistry and Physics*, 16(2):691–701.

[van der Dussen, 2014] van der Dussen, S. R. d. R. (2014). An LES model study of the influence of the free tropospheric thermodynamic conditions on the stratocumulus response to a climate perturbation. pages 670–691.

[Wood, 2012] Wood, R. (2012). Stratocumulus Clouds. *Monthly Weather Review*, 140(8):2373–2423.

[Wood and Bretherton, 2004] Wood, R. and Bretherton, C. S. (2004). Boundary layer depth, entrainment, and decoupling in the cloud-capped subtropical and tropical marine boundary layer. *Journal of Climate*, 17(18):3576–3588.

[Young, 1988] Young, G. S. (1988). Turbulence structure of the convective boundary layer. Part II: Phoenix 78 aircraft observations of thermals and their environment.